4-2021

Variation in the Genome and Transcriptome Associated with Beef Cattle Production and Investigation of the Metabolic Consequences of Beta-adrenergic Agonist Supplementation

Renae L. Sieck
University of Nebraska - Lincoln, renae.sieck@huskers.unl.edu

VARIATION IN THE GENOME AND TRANSCRIPTOME ASSOCIATED WITH BEEF CATTLE PRODUCTION AND INVESTIGATION OF THE METABOLIC CONSEQUENCES OF BETA-ADRENERGIC AGONIST SUPPLEMENTATION

by

Renae L. Sieck

A THESIS

Presented to the Faculty of

The Graduate College at the University of Nebraska

In Partial Fulfillment of Requirements

For the Degree of Master of Science

Major: Animal Science

Under the Supervision of Professor Jessica L. Petersen

Lincoln, Nebraska

April 2021

VARIATION IN THE GENOME AND TRANSCRIPTOME ASSOCIATED WITH BEEF CATTLE PRODUCTION AND INVESTIGATION OF THE METABOLIC CONSEQUENCES OF BETA-ADRENERGIC AGONIST SUPPLEMENTATION

Renae Lyn Sieck, M.S.

University of Nebraska, 2021

Advisor: Jessica L. Petersen

Beta-adrenergic agonists (β-AA) are widely used supplements in livestock production to improve feed efficiency and increase lean muscle mass. Heat stress is one of the largest economic burdens to the livestock industry due to production efficiency losses and morbidity and mortality of animals. Both β-AA and catecholamines released in response to heat stress bind to β-adrenoceptors on the skeletal muscle cell surface to activate downstream signaling pathways. The purpose of this study was to determine if β-AA supplementation and heat stress have an additive effect on the skeletal muscle transcriptome. 3' RNA sequencing of samples of the *longissimus dorsi* was performed to quantify gene expression and identify genes differentially expressed due to treatment. No additive effects were observed, but instead β-AA supplementation mediated the heat-stress induced oxidative stress response in skeletal muscle. Therefore, the objective of the second study was to identify the influence of β-AA on mitochondrial function in skeletal muscle satellite cells of cattle, sheep, and pigs. Real-time measurements of oxygen consumption rates were recorded using intracellular flux analysis. Incubation of bovine cells with β-AA increased maximal respiration and spare respiratory capacity ($P<0.05$). No measures of mitochondrial function were altered by β-AA in ovine or porcine cells.

These findings indicate that β-AA improve the efficiency of bovine muscle stem cells in part by modifying mitochondrial function.

The third study identified genomic variation underlying a congenital facial deformity in Hereford cattle termed Mandibulofacial Dysostosis (MD). Affected calves shared hallmark features of a variably shortened and/or asymmetric lower mandible and bilateral skin tags caudal to the commissure of the lips. Whole genome sequencing led to the discovery of a missense variant (Chr26 g. 14404993T>C) in *CYP26C1* associated with MD. We postulate that this recessive missense mutation impacts the catalytic activity of the encoded enzyme, leading to the observed MD phenotype.

AKNOWLEDGEMENTS

To my advisor Dr. Jessica Petersen: I greatly appreciate the opportunity you made for me to work on projects that I loved. Your willingness to challenge me to grow and learn has led me to accomplish things that I did not know were possible. Thank you for believing in my abilities and encouraging me along the way.

I greatly appreciate all the members of our lab group who have helped me the last two years. To our lab manager Anna Fuller: Thank you for supporting me not only on lab procedures, but also as a friend. I greatly appreciate your willingness to be my problem solver and idea generator. To Leah Treffer: I am very thankful for your hard work and patience with me when I make mistakes, especially as we endured some learning curves together. I appreciate that you made days in the cell lab fun. To Rachel Reith: Thank you for putting in long hours with me during our research trials and for being willing to explore with me when we traveled. Our national park trips were some of my favorite adventures of graduate school. I am glad that we were study partners and that we taught each other new things. To Pablo Grijalva: I appreciated that you brought laughs to trial days and that you introduced us to the best food in Tucson. To Alexa Barber: I greatly appreciate your willingness to help with my projects in whatever way you could. I have enjoyed our chats about lab work and life.

To my family and friends: I could not have completed my research projects and thesis writing without your emotional support. Thank you for believing in me and encouraging me in every way possible.

GRANT INFORMATION

Projects 1 and 2 are based on research that was partially supported by the Nebraska Agricultural Experiment Station with funding from the Hatch Multistate Research capacity funding program (Accession Number 1011055) from USDA National Institute of Food and Agriculture.

Project 3 was funded in part by the American Hereford Association, agreement 130363.

TABLE OF CONTENTS

CHAPTER 1: LITERATURE REVIEW

Part I: Livestock Efficiency and Stress

β-Adrenergic Agonist Introduction

β-adrenergic cell signaling is initiated with the binding of epinephrine, norepinephrine, or an exogenous agonist to G-protein coupled β-adrenoceptors (Mersmann, 1998). When bound, the G_s protein α-subunit activates adenylate cyclase, which converts ATP to 3',5'-cyclic adenosine monophosphate (cAMP) (Mersmann, 1998; Cairns and Borrani, 2015). This second messenger is responsible for signal transduction to multiple cAMP-dependent protein kinases (PKA) whose role is to phosphorylate target proteins (Cairns and Borrani, 2015); phosphorylation by PKA can either activate or repress these protein targets. An example of activation is phosphorylation of hormone sensitive lipase, which actives triacylglycerol degradation in adipocytes (Mersmann, 1998). On the other hand, inactivation of acetyl-CoA carboxylase occurs by phosphorylation during long chain fatty acid biosynthesis (Mersmann, 1998). PKA can also regulate transcription by phosphorylating the cAMP response binding protein (CREB). This protein interacts with cAMP Response Element (CRE), a DNA sequence near the promoter of target genes to activate transcription (Mersmann, 1998).

There are three known subtypes of β-adrenoceptors (β-AR), the prevalence of which differs by tissue and among species (Mersmann, 1998). Cattle skeletal muscle has predominantly β_2-AR, but β_1-AR and a small portion of β_3-AR are also present (Sillence

and Matthews, 1994). Alternatively, pig skeletal muscle has primarily the β_1-AR subtype with a smaller number of β_2-AR and an even smaller proportion of β_3-AR (McNeel and Mersmann, 1999). Receptor subtype abundance has not been explicitly studied in sheep but trials in which sheep are supplemented with either a β_1- or β_2-AA have resulted in a more robust response to the β_2-AA; sheep skeletal muscles are therefore presumed to have primarily the β_2-AR subtype similar to cattle (Lopez-Carlos et al., 2011). β-AA that have been used as feed supplements in the livestock industry are able to bind to multiple receptor subtypes. Zilpaterol HCl (ZH) can bind both subtypes but has a greater affinity for the β_2-AR (Verhoeckx et al., 2005). Ractopamine HCl (RAC) has a similar affinity for both the β_1-AR and β_2-AR (Mills, 2002).

β-Adrenergic Agonist Cattle Production Outcomes

Supplementation of β-AA to livestock species improves multiple production outcomes. ZH has a significant effect on both live weight and hot carcass weight (Elam et al., 2009). A meta-analysis across 31 studies of ZH feeding trials identified that, on average, carcass weight and live weight are increased (15 kg and 8 kg respectively) in supplemented steers relative to non-supplemented controls (Lean et al., 2014). This difference can be attributed to ZH supplemented steers having a 1.7% higher dressing percentage on average (Lean et al., 2014). ZH supplementation alters both intramuscular and intermuscular fat deposition by decreasing 12^{th} rib fat and decreasing marbling score (Lean et al., 2014). These changes in fat deposition decrease the percentage of carcasses with a Prime or Choice USDA quality grade in both ZH supplemented heifers and steers

(Elam et al., 2009; Rathmann et al., 2012). Still, ZH supplementation provides value for cattle selling on the grid because yield grades are decreased (Elam et al., 2009; Rathmann et al., 2012). Additionally, ZH adds value to beef carcasses because loin muscle area is increased (Elam et al., 2009). ZH supplementation also improves cattle performance before harvest. ZH supplemented heifers had increased average daily gain and decreased dry matter intake resulting in an improved gain to feed ratio between ZH supplemented heifers and controls (Montgomery et al., 2009; Rathmann et al., 2012). Similar studies in steers supplemented with ZH did not report a significant difference in dry matter intake, but did report significant changes in average daily gain and gain to feed ratio (Vasconcelos et al., 2008; Elam et al., 2009).

Zilpaterol was approved by the FDA for use as a growth promoter in cattle in 2006 (U.S. Food and Drug Administration (FDA), 2006). However, in the summer of 2013 anecdotal evidence linked ZH supplementation to impairment of mobility in cattle upon arrival to harvest facilities (Thomson et al., 2015). A subsequent study evaluated steers under heat stress found no significant impact of ZH on animal mobility (Boyd et al., 2015). No subsequent studies have provided further evidence supporting the anecdotal mobility impairment (Marti et al., 2021).

Ractopamine, approved for use in cattle in 2003, has similar effects on cattle production traits as ZH but to a lesser magnitude (Lean et al., 2014). Multiple studies reported that RAC improved average daily gain and gain to feed ratio, increased hot carcass weight and loin muscle area, but did not change dressing percentage, fat thickness, and yield grade between controls and supplemented steers (Gruber et al., 2007; Winterholler et al., 2007). Another study found that RAC increased body weight, average

daily gain, feed efficiency, and hot carcass weight compared to controls. However, RAC did not influence carcass composition (Scramlin et al., 2010). In some cases, RAC supplementation induced changes in feed efficiency but did not influence carcass characteristics or body weight (Quinn et al., 2008). RAC continues to be fed as a supplement for feedlot cattle.

β-Adrenergic Agonist Physiological Mechanisms

One mechanism by which β-AA increase loin muscle area in supplemented animals is by inducing muscle hypertrophy. In lambs, ZH supplementation increased cross-sectional muscle fiber areas compared to controls while the ratio of Type 1 and Type 2 fibers and the amount of MyHC-I and MyHC-II protein did not change (Barnes et al., 2019). There was no evidence of RAC induced muscle hypertrophy in these lambs (Barnes et al., 2019). There was also no change in the proportion of MyHC-I, MyHC-IIA, and MyHC-IIX fibers in ovariectomized beef heifers supplemented ZH (Hergenreder et al., 2017) The authors also reported that ZH supplementation decreased the amount and cross-sectional area of MyHC-1 fibers while increasing the amount and cross-sectional area of MyHC-IIX fibers (Hergenreder et al., 2017). Further, ZH supplementation and an estrogen and trenbolone acetate implant resulted in an additive effect on increased fiber cross-sectional area (Kellermeier et al., 2009). It is therefore well documented that ZH increases muscle hypertrophy by increasing cross-sectional area of some muscle fiber types with little change in the proportion of the fiber types.

There are conflicting data regarding whether RAC supplementation increases the cross-sectional area of muscle fibers. Some studies found no difference in fiber cross-sectional area when comparing RAC-supplemented animals and controls (Gonzalez et al., 2010; Barnes et al., 2019). Others reported that RAC increased the Type I and Type IIA fiber cross-sectional area in cattle (Gonzalez et al., 2007) and Type IIX fiber cross-sectional area in pigs (Li et al., 2015). The effect on Type I fibers was additive in combination with trenbolone acetate plus estradiol implants (Gonzalez et al., 2008). These results indicate that increases in fiber cross-sectional area are likely not the only mechanism by which RAC increases carcass weight and loin muscle area.

Alternatively, muscle hypertrophy in RAC-supplemented animals may also be induced by an alteration in muscle protein synthesis rates. In cultured rat myotubes, RAC supplementation increased the muscle protein synthesis rate as indicated by greater myosin heavy chain protein than in controls. This effect was further amplified due to no changes in protein degradation between treatments (Anderson et al., 1990). Protein synthesis also plays a role in muscle hypertrophy of livestock animals. In finishing pigs, RAC supplementation resulted in increased fractional protein synthesis in the *semitendinosus*, *longissimus dorsi,* and *biceps femoris* muscles. Again, protein breakdown was similar between control and supplemented pigs. (Bergen et al., 1989; Adeola et al., 1992). These muscles result in high-value meat cuts, so hypertrophy adds retail value. No studies have reported the effects of RAC on protein synthesis rates in ruminants, but this mechanism is also plausible in these species.

Another possible mechanism of muscle hypertrophy is an increased rate of satellite cell proliferation, differentiation, and fusion with existing muscle fibers resulting

in a greater number of nuclei in the muscle (Gonzalez et al., 2007). There are variable results of the impact of β-AA on nuclei density in skeletal muscle, but multiple studies provide evidence that this is not the mechanism of action for muscle hypertrophy in β-AA supplemented animals. Decreased total nuclei density has been reported due to either ZH supplementation (Hergenreder et al., 2017) or RAC supplementation (Gonzalez et al., 2008). Other studies reported no change in nuclei density (Gonzalez et al., 2007).

Beta-adrenergic agonists also influence cattle efficiency by altering cellular glucose oxidation. In one study, glucose oxidation increased by approximately 32% in ZH stimulated soleus muscle strips of Sprague-Dawley rats. This response was independent of insulin activity and glucose uptake, indicating greater metabolic efficiency of β_2-AA treated muscle strips (Cadaret et al., 2017). Similarly, glucose oxidation rates were approximately 15% greater in muscle strips isolated from ZH supplemented lambs than non-supplemented animals (Barnes et al., 2019). Together these studies provide preliminary evidence for a mechanism by which β-AA improve cellular efficiency that could result in the production outcome of increased feed efficiency.

Ractopamine is only supplemented for the last 28 to 42 days of the cattle finishing phase (U.S. Food and Drug Administration (FDA), 2020). A physiological explanation underlying this rule is that overstimulation leads to β-AR desensitization (Waldo et al., 1983; Lohse et al., 1990). One mechanism of desensitization is the internalization of the β-AR due to endocytosis leading to a reduced ability of the receptor to stimulate adenylate cyclase (Lefkowitz et al., 1983). Supporting this assertion, ZH increased the proportion of internalized β_2-AR in beef heifers (Hergenreder et al., 2017). Further, supplementation increased β_2-AR mRNA abundance in the skeletal muscle of heifers and

steers, potentially to replace internalized receptors (Sissom et al., 2007; Winterholler et al., 2007). However, increased receptor abundance is not consistently reported. RAC decreased both β_1-AR and β_2-AR mRNA abundance in Holstein steers (Walker et al., 2007), decreased β_2-AR mRNA abundance in pigs (Gunawan et al., 2007), and there was no effect of β-AA on β-AR abundance in beef heifers (Hergenreder et al., 2017). The timing of the maximal response has not been studied in ruminants, but pigs supplemented β-AA had a maximal growth response 7 to 10 days after supplementation was initiated, with the response decreasing to about zero within six weeks (Mills, 2002).
Together these results provide evidence that feeding β-AA longer than the FDA recommendation would not provide additional benefit in cattle production outcomes.

The effects of β-AA on the muscle transcriptome vary across livestock species and supplement type. Since the adrenergic system is typically associated with the stress response, the whole blood transcriptome of cattle supplemented RAC was studied for evidence of systemic inflammation, but none was identified. However, genes involved in inflammatory pathways were upregulated including *IFI35*, *TYROBP*, and *TP53INP1* (Burrack et al., 2020). Alteration of the abundance of transcripts associated with the skeletal muscle stress response were also reported in RAC supplemented pigs (Brown et al., 2018), and RAC supplementation altered pathways associated with muscle metabolism in pigs (Brown et al., 2018). This may not be the case in ruminants because RA supplementation resulted in no differentially expressed (DE) genes in feedlot lambs (Kubik et al., 2018). These transcriptomic differences may indicate a cellular mechanism by which pigs have a greater phenotypic response to RAC than ruminants. Alternatively, ZH supplementation alters transcripts associated with muscle growth and metabolism in

ruminants. DE genes in feedlot lambs were associated with muscle hypertrophy and muscle oxidative metabolism (Kubik et al., 2018). In Holstein steers, RAC increased expression of *IGF-1* in the *longissimus dorsi* muscle (Walker et al., 2007). These studies indicate that further research is warranted to identify how to transcriptome is altered by β-AA supplementation; studies are particularly lacking in beef cattle.

Mitochondrial Role in Livestock Efficiency

Increasing the efficiency of production is a way producers are working to improve the sustainability of the livestock industry. Feed efficiency is one measurable outcome producers seek to improve to enhance overall production efficiency. Multiple factors contribute to feed efficiency in livestock animals including feed intake, fermentation and digestion, postabsorptive metabolism, physical activity of the animal, and thermoregulation (Derno et al., 2019). Animal differences in feed efficiency can be described by differences in these basal factors, but also by variation in the animals' physiological response to external factors including feed supplements or environmental stress. Mitochondria play an essential role in post-absorptive metabolism and therefore have been a focus of studies looking to optimize livestock production efficiency.

ATP production via oxidative phosphorylation (OXPHOS) is a system made up of over 85 proteins (Smeitink et al., 2001). Additional complexity is added when thirteen of these proteins are encoded by the maternally inherited mitochondrial genome and the others are encoded by the nuclear genome. The OXPHOS system contains 5 enzyme complexes (I-V) and two carriers of electrons (coenzyme Q and cytochrome c) whose

role is to produce ATP via the formation of a proton gradient across the inner mitochondrial membrane (Smeitink et al., 2001). Substrates are oxidized in the tricarboxylic acid cycle where NADH and $FADH_2$ are produced (Salin et al., 2015). The role of the cofactors is to pass electrons on to the protein complexes of the electron transport chain. These complexes establish an electrochemical gradient across the inner mitochondrial membrane. This gradient is required for Complex V (ATP synthase) to produce cellular energy by phosphorylating ADP to ATP (Salin et al., 2015).

Mitochondria provide over 90% of cellular ATP, therefore animal performance is impacted by mitochondrial efficiency (Bottje and Carstens, 2009). Efficiency can be measured as the ratio of ATP generated per molecule of oxygen consumed. There is a significant amount of variation in this measure between individuals, populations, environments, and within a single individual over time (Salin et al., 2015). At a cellular level this variation is caused by substrate type at the beginning of oxidative phosphorylation, the efficiency of proton pumps located on the mitochondrial inner membrane, or uncoupling of the electron transport chain (ETC) from ATP production as a result of proton leak (Salin et al., 2015). Proton leak causes the most variation in mitochondrial efficiency. It has been estimated that mitochondrial proton leak is responsible for approximately 20% of the basal energy expenditure of an animal (Bottje and Carstens, 2009). Supporting the role of mitochondrial efficiency in production, beef steers with a low residual feed intake had greater coupling between the ETC and ATP production than steers with a high residual feed intake (Kolath et al., 2006). Poultry studies have also demonstrated that high growth efficiency birds had reduced proton leak

relative to less efficient animals (Toyomizu et al., 2011). These factors indicate that mitochondrial efficiency plays a crucial role in overall animal efficiency.

Multiple factors play a role in the coupling or uncoupling of oxygen consumption to ATP production. The primary environmental factor influencing mitochondrial efficiency of mammals is chronic cold stress where uncoupling results in increased heat production by the mitochondria as a mechanism to aid in thermoregulation (Salin et al., 2015). Also, reduced feed intake often results in increased ATP generated per molecule of oxygen resulting in decreased oxygen consumption necessary to maintain homeostasis (Salin et al., 2015). To compensate for ATP expenditure during muscle contraction, mitochondria accelerate metabolic rate and ATP turnover. Cells respond in a similar manner when there is uncoupling of the electron transport chain and a decreased efficiency of respiration (Adhihetty et al., 2003). In poultry animals with high growth efficiency, there was less expression of proteins associated with uncoupling of oxygen consumption with ATP production in muscle mitochondria than less efficient animals (Toyomizu et al., 2011). These studies provide further evidence that mitochondrial function is essential to overall feed efficiency in livestock.

Given the effects mitochondrial efficiency plays in animal efficiency, one could assume that selection pressure over time would have resulted in maximal efficiency of the mitochondria. However, increasing ATP production per oxygen consumed also results in an increase in Reactive Oxygen Species (ROS) generation (Salin et al., 2015). ROS are any oxygen-containing reactive species, including superoxide and hydrogen peroxide (Li et al., 2016). ROS typically interact with antioxidants in the body and homeostasis is maintained, but when ROS production is greater than antioxidant

production, cells are in oxidative stress (Li et al., 2016). This type of cellular stress can lead to damage of lipids, proteins, and nucleic acids and can compromise overall cellular survival (Salin et al., 2015). ROS production in livestock species is linked to both biological factors such as diseases and external factors such as heat stress (Mujahid et al., 2007; Celi, 2011),

Oxidative stress is detrimental to livestock feed efficiency. Low feed efficiency broilers had a greater amount of protein damage caused by ROS than higher feed efficiency animals indicating a greater amount of oxidative stress in the less feed efficient birds. The same effect was described in low feed efficiency steer muscle mitochondria (Bottje and Carstens, 2009). Additionally, a positive correlation between residual feed intake and ROS production in the mitochondria of pig muscle has been reported; more feed-efficient animals had less ROS in skeletal muscle (Grubbs et al., 2013). These studies provide evidence that decreased feed efficiency in livestock species can be attributed to mitochondrial dysfunction via ROS production, and increased feed efficiency can be attributed to improved metabolic function.

Heat Stress Introduction

Heat stress, a greater heat load than capacity for heat dissipation (Bernabucci et al., 2010), is one of the largest economic burdens to the livestock industry due to production efficiency losses and morbidity and mortality of animals (St-Pierre et al., 2003). When an animal is subjected to heat stress they have increased energy required for maintenance (Beede and Collier, 1986) and nutrients are diverted from protein synthesis

to thermoregulation (Ross et al., 2015). In addition to production deficits through a reduction in efficiency, heat-induced morbidity and mortality takes place when the body temperature rises approximately 3ºC to 4ºC (Bernabucci et al., 2010). Moderating the effects of heat stress is of high interest to improve livestock production efficiency and animal well-being.

Heat Stress Cattle Production Outcomes

The most prominent production outcomes as a result of heat stress are decreased feed intake, increased water intake, increased respiration rate, and increased body temperature (Bernabucci et al., 2010). Cattle eat less when the ambient temperature is high as an adaptive mechanism to reduce metabolic heat production (Gonzalez-Rivas et al., 2020). This effect begins to take place in beef cattle when temperatures exceed 30ºC and 80% relative humidity (Bernabucci et al., 2010). Decreased feed intake is also detrimental to average daily gain and carcass weight in heat-stressed heifers (Mitlöhner et al., 2001), results in decreased muscle mass in pigs (Ross et al., 2015), and decreased average daily gain, feed conversion ratio, and breast and thigh muscle weight of broilers compared to pair-fed controls (Zuo et al., 2015). Another thermoregulatory response to heat stress is increased water intake. Some animals consume twice the amount of water during heat stress than they consume in thermoneutral conditions (Beede and Collier, 1986). Additional water helps cool cattle by decreasing digestive tract temperature and through evaporative cooling via sweating and panting (Beede and Collier, 1986). Heat stress can also be detrimental to meat quality if it persists immediately prior to harvest.

Pre-harvest heat stress in cattle can lead to dark firm and dry meat because of low muscle glycogen reserves that result in high muscle pH. Feedlot cattle consuming diets with rapidly fermentable grains are the most susceptible to this outcome (Gonzalez-Rivas et al., 2020).

The physiological response to heat stress is not consistent over time and can be mediated in certain cases. There is evidence that the effect of heat stress on broilers is time-dependent. Chickens that were heat stressed for one week had reduced average daily gain and average daily feed intake relative to controls. After two weeks of heat stress, the groups were no longer significantly different in these measures indicating acclimation of the heat stressed birds to the environment (Wang et al., 2019). Additionally, providing cattle with shade mediates the negative effects of heat stress on animal performance and carcass characteristics (Mitlöhner et al., 2002). Sprinkler systems are also utilized to improve physiological indicators of stress in cattle (Marcillac-Embertson et al., 2009). For livestock such as pigs and poultry that are housed in barns, air treatment devices aid in heat stress mitigation (Vitt et al., 2017). Overall, these results show that the detrimental impacts of heat stress on animal performance can be reduced with changes in an animal's environment or with physiological adaptations to that environment.

Physiological Mechanisms of Heat Stress

Traditionally, production losses due to heat stress have been attributed to reduced feed intake, but recent studies with pair fed animals have revealed additional physiological mechanisms that play a role in the production loss. These include

alterations in protein synthesis, muscle metabolism, inflammatory signaling, and mitochondrial function.

Alterations in protein synthesis have been reported in ruminants, pigs, and poultry. Broilers that were heat stressed for two weeks had altered body composition compared to controls with decreased protein gain and retention (Geraert et al., 1996). The underlying genomic cause of decreased protein synthesis in broilers was attributed to decreased expression of *IGF-1*, *p70S6K,* and *PIK3*; increased protein degradation was attributed to increased expression of the degradation-associated genes *MuRF1* and *MAFbx* in breast muscle (Zuo et al., 2015). Decreased protein synthesis was also reported in gilts under 12-hour acute heat stress (Ganesan et al., 2018). Chronic heat stress in pigs also caused transcriptome changes in the *longissimus dorsi* muscle of pigs with reported downregulation of 11 genes important for muscle growth, structure, and function (Yue Hao et al., 2016). The same effect was reported in ruminants where hyperthermia resulted in decreased protein synthesis and increased muscle catabolism (Baumgard and Rhoads, 2013). Together these results indicate that alterations in protein synthesis and maintenance in muscle is one physiological mechanism by which heat stress decreases muscle mass in livestock.

Heat stress negatively alters mitochondrial function by inducing mitochondrial damage (Ganesan et al., 2016). Gilts that underwent heat stress for 12 hours showed signs of increased oxidative stress in oxidative but not glycolytic muscle (Ganesan et al., 2017). However, the effects of oxidative stress in pig skeletal muscle may be limited to an acute response because another study reported signs of oxidative stress in oxidative muscle after one day of heat stress but not after three, and no changes in glycolytic muscle

(Montilla et al., 2014). A time-dependent response in ROS production due to heat stress was also reported in broilers where ROS was increased in skeletal muscle after one week, but after two weeks of heat stress ROS production did not differ between heat stressed birds and controls (Wang et al., 2019). Observations of oxidative stress in oxidative muscle but not glycolytic muscle is evidence that the ROS causing the oxidative damage originate from alterations in mitochondrial function (Ganesan et al., 2017). Chickens under acute heat stress had increased ROS in skeletal muscle mitochondria due to enhanced substrate oxidation (Mujahid et al., 2005; Mujahid et al., 2007). Another study in broilers found that ROS was increased at day 3, 5 and 9 of heat stress but returned to original levels by day 14. They concluded that the increase in ROS can be attributed to increased mitochondrial oxygen consumption during acute heat stress (Azad et al., 2010). Transcriptomic analysis of sheep skeletal muscle provides further evidence of an oxidative stress response given upregulation of genes related to this process (Kubik et al., 2018). Further supporting the conclusion that heat stress induces oxidative stress in livestock skeletal muscle, supplementation of antioxidants to sheep mediated the negative impacts of heat stress induced ROS (Chauhan et al., 2014). These studies provide evidence that heat stress induces an acute increase in ROS production in skeletal muscle due to increases in mitochondrial function.

There is inconclusive evidence of the effect of heat stress on mitochondrial content in oxidative skeletal muscle. Mitochondrial content was increased in the oxidative skeletal muscle of heat stressed gilts (Ganesan et al., 2017) but was not altered in another gilt study (Volodina et al., 2017). One plausible mechanism for increased mitochondrial content in heat stressed oxidative muscle is failure of the cell to remove

mitochondria that have been damaged by ROS with no alterations in mitochondrial biogenesis (Ganesan et al., 2017). This mechanism is supported by evidence that heat stress reduces autophagy and autophagosomal degradation of damaged mitochondria (Brownstein et al., 2017).

Heat stress induces inflammatory signaling in skeletal muscle but acts differently between oxidative and glycolytic fibers. In gilts, acute heat stress caused inflammatory signaling through the NF-kB pathway of oxidative muscle, but no signs of inflammation were present in glycolytic muscle (Ganesan et al., 2016). No signs of inflammatory signaling, however, were reported after 1 or 3 days of heat stress another set of gilts (Montilla et al., 2014). In sheep, heat stress increased the expression of NF-kB and TNF-α, indicating dysregulation of the muscle inflammatory response, but the effect was also mitigated by the supplementation of an antioxidant (Chauhan et al., 2014). These data indicate that the timing and mechanism of the inflammatory response to heat stress in muscle are not fully understood.

Physiological Outcomes of β-AA and Heat Stress Interactions

The adrenergic system is typically associated with the stress response. Epinephrine and norepinephrine regulate the animal's physiological response to heat stress by increasing respiration rate, heart rate, body temperature, blood flow to the skin for thermoregulation, and muscle glycogenolysis while decreasing glycogenesis (Gonzalez-Rivas et al., 2020). β-AA supplementation is a vital strategy to increase livestock efficiency, however since β-AA bind to the same receptor as epinephrine and

norepinephrine on the cell surface, it is important to determine if any additive effects exist between these supplements and other additional stress sources. Multiple studies reported that β-AA supplemented livestock had decreased body temperatures compared to controls. This decreased body temperature was reported during heat stress although the ZH supplemented steers had increased respiration rates indicating that β-AA helped mediate the effect of the heat stress (Boyd et al., 2015). The decreased body temperature was also reported in ZH supplemented heifers that underwent an endocrine stress (Buntyn et al., 2016). A plausible mechanism for the decreased body temperature is that β-AA act as vasodilators (Dawes Matthew et al., 1997); β-AA supplemented animals may therefore more easily dissipate heat (Buntyn et al., 2016). β-AA mediation of stress was also reported in ZH supplemented heifers due to decreased cortisol and epinephrine levels in the blood relative to non-supplemented controls after an endocrine stress challenge (Buntyn et al., 2016). This indicates a possible downregulation of aspects of the hypothalamic-pituitary-adrenal axis due to ZH supplementation.

Part II: Molecular Regulation of Mandible Development

The proteome is cell type specific, resulting in differing biological functions of cells. A primary regulator of the specificity of proteins found in cells are transcription factors that function as promoters, enhancers, insulators, and silencers (Lee et al., 2012). Multiple transcription factors are associated with muscle growth and development (Ludolph and Konieczny, 1995). External stressors, such as heat stress, alter the profile of active transcription factors in muscle resulting in changes in the functional proteins

present in the cell (Xie et al., 2014). The abundance of cellular protein can also be altered by variants in the genome, which can alter transcription factor binding to DNA, resulting in changes in DNA transcription (Johnston et al., 2019). Additionally, loss of function variants in the exons of genes can result in dysfunctional proteins. Each of these mechanisms alter the proteome with the ability to disrupt essential components of cellular function.

Deleterious syndromes in livestock species can be attributed to variants inherited in a Mendelian manner. Over 250 Mendelian traits in cattle are reported in the Online Mendelian Inheritance in Animals database (https://omia.org/home). Often, deleterious syndromes in cattle are attributed to variants inherited in an autosomal recessive manner (Ciepłoch et al., 2017). Due to this inheritance pattern, clinical signs of disease may not appear for many generations after the causal mutation originates. However, artificial selection in livestock and the commonplace use of artificial insemination and embryo transfer can expedite widespread proliferation of a deleterious variant. The significant impact of a single deleterious variant in livestock can be exemplified by a recessively inherited mutation in *APAF1*, traced back to a Holstein bull born in 1962. The recessive genotype, detrimental to cow fertility, was estimated to have resulted in 525,000 abortions costing the industry $420 million (Adams et al., 2016). In beef cattle, congenital abnormalities affect a wide range of tissues including the eyes, nervous system, skin, muscle, skeleton and blood (Ciepłoch et al., 2017). Genetic testing is a vital tool to avoid these detrimental phenotypes in livestock. For these tests to be developed, it is vital that producers report congenital abnormalities so that the inheritance pattern and genomic variants underlying the abnormality can be identified.

Recessively inherited genetic variants also underly craniofacial defects in cattle. For instance, a frameshift in *ZIC2* resulted in frontonasal dysplasia in a Limousin calf (Braun et al., 2021) and facial dysplasia syndrome in Holstein cattle was attributed to a dominantly inherited missense mutation in *FGFR2* (Agerholm et al., 2017). Holstein cattle affected by hypotrichosis with anodontia have no, or deformed teeth, and significant hair loss. This condition has been attributed to an x-linked recessively inherited deletion in *ED1* (Drögemüller et al., 2002). Additional congenital abnormalities resulting in cleft palate or short lower jaws have been reported in various cattle breeds, but molecular mechanisms underlying the conditions have not been elucidated (Gentile and Testoni, 2006). Therefore, the molecular regulation of mandible development in cattle is not fully understood.

The population of embryonic neural crest cells that eventually give rise to the muscles and bones of the face are referred to as cranial neural crest cells (CNCC). These cells originate in the neural tube then migrate to their destination in the cranial region of the developing embryo. Upon arrival, further subdivision into region-specific groups is regulated by gradients of multiple cellular signals including FGF, retinoic acid, and WNT (Williams and Bohnsack, 2019). Proliferation of CNCC gives rise to the pharyngeal arches (Parada and Chai, 2015). Further functional specification of CNCC in the first pharyngeal arch (PA-1) is regulated by the distal-less (Dlx) family of genes. Two of these, *Dlx1* and *Dlx2,* are expressed in both the maxillary and mandibular process of PA-1. *Dlx5* and *Dlx6* are expressed only in the mandibular process near the future fusion site of the mandible and maxilla. Finally, *Dlx3* and *Dlx4* are expressed in the most distal end of the mandibular process (Depew et al., 2005). Regulation of Dlx gene expression in

PA-1 is controlled by the Endothelin-1 (ET-1) signaling pathway (Gitton et al., 2010) where it activates expression of *Dlx5* and *Dlx6* (Vieux-Rochas et al., 2007; Williams and Bohnsack, 2019). CNCC in the maxillary prominence develop into the upper lip and maxilla while the mandibular prominence gives rise to the mandible and tongue (Parada and Chai, 2015). CNCC located in the mandibular process condense and organize into Meckel's cartilage (MC). This cartilage extends from the fusion site of the mandible and maxilla to the middle ear (Parada and Chai, 2015). MC serves as a scaffold during intramembranous ossification of the mandible bone. The proximal end of MC forms the malleus and incus bones and the remaining portion of MC is degraded (Vieux-Rochas et al., 2007; Parada and Chai, 2015).

Retinoic acid (RA) is an active metabolite of vitamin A and is essential to normal development due to its role in transcriptional regulation of over 530 genes including those involved in CNCC migration and differentiation (Kedishvili, 2013; Williams and Bohnsack, 2019). Dysregulation of RA can cause a wide array of congenital abnormalities that are dependent on the spatial and temporal regulation of RA during development (Gitton et al., 2010; Kedishvili, 2013; Williams and Bohnsack, 2019). RA is a repressor of ET-1. (Vieux-Rochas et al., 2007; Williams and Bohnsack, 2019). Decreased ET-1 expression results in decreased expression of *DLX5* and *DLX6*, genes that regulate MC development (Vieux-Rochas et al., 2007). Since MC is transient, RA regulation of its formation is also highly time point specific. Embryo exposure to RA treatment at 9 somites results in alterations of MC development (Gitton et al., 2010). This is the time point when CNCC reach PA-1 (Vieux-Rochas et al., 2007). Excess RA during development has resulted in craniofacial abnormalities including microtia, cleft palate,

cleft lip, and micrognathia (Williams and Bohnsack, 2019). RA treatments in mice resulted in loss of the distal portion of MC (Vieux-Rochas et al., 2007).

A primary source of retinol in a cattle diet is from β-carotene in plants. Once in the small intestine β-carotene is cleaved into all-trans-retinaldehyde. This molecule is then further oxidized into all-trans-retinoic acid due to the enzymatic action of *RALDH1, RALDH2,* and *RALDH3* (Williams and Bohnsack, 2019). RA is degraded by enzymes transcribed from another gene family including *CYP26A1, CYP26B1,* and *CYP26C1* (Kedishvili, 2013; Williams and Bohnsack, 2019). During embryo development, the CYP26 family enzymes are expressed in a spatially specific manner (Tahayato et al., 2003). *CYP26C1* is expressed in the maxillary and mandibular components of PA-1 when CNCC reach the region (Tahayato et al., 2003; Vieux-Rochas et al., 2007; Gitton et al., 2010). Other CYP26 family genes are expressed thought the animal's life but *CYP26C1* expression is restricted to embryonic development (Guengerich, 2015). *CYP26C1* also expresses greater substrate specificity than other genes in the CYP26 family (Kedishvili, 2013).

Congenital abnormalities in humans have been attributed to mutations in *CYP26C1*. A condition termed Focal Facial Dermal Dysplasia type 4 is specifically attributed to multiple different variants in *CYP26C1.* This condition is characterized by congenital scar-like lesions located near the fusion site of the mandibular and maxillary prominences. Affected individuals are typically otherwise considered developmentally normal (Slavotinek et al., 2013; Lee et al., 2018). *CYP26C1* has also been implicated as a genetic modifier in idiopathic short stature (Montalbano et al., 2016).

An understanding of the genomic regulation of development is vital for identifying variants underlying inherited abnormalities. Additionally, livestock models provide new avenues to study human disease due to more similar size and homology than other model organisms (Bassols et al., 2014). Progress in our understanding of the genes involved in inherited developmental abnormalities will aid in the prevention and treatment of these conditions in humans and livestock.

CHAPTER 2: TRANSCRIPTOME EFFECTS DUE TO β-ADRENERGIC AGONIST SUPPLEMENTATION AND HEAT STRESS

Introduction

Heat stress is one of the largest economic burdens to the livestock industry due to production efficiency losses and morbidity and mortality of animals. In the beef industry alone, heat stress results in an estimated annual cost of $369 million (St-Pierre et al., 2003). Heat stress causes a decrease in average daily gain and dry matter intake in cattle (Mitlöhner et al., 2001). This is in part due to an adaptive mechanism to reduce heat production during digestion (Basarab et al., 2003). Epinephrine and norepinephrine regulate the animal physiological response to heat stress in part by binding to β-AR to activate downstream signaling pathways (Gonzalez-Rivas et al., 2020). In skeletal muscle, heat stress decreases protein synthesis and increases muscle catabolism (Baumgard and Rhoads, 2013). Acute heat stress also results in oxidative stress in skeletal muscle due to increased reactive oxygen species production (Azad et al., 2010; Ganesan et al., 2017).

β-adrenergic agonists (β-AA) are feed supplements commonly used in the livestock industry. The β_1-AA Ractopamine (RAC) and β_2-AA Zilpaterol HCl (ZH) improve cattle growth performance, carcass weight, and *longissimus dorsi* muscle area during the finishing phase (Elam et al., 2009; Lean et al., 2014). β-AA also change carcass composition by altering both intramuscular and intermuscular fat deposition. ZH supplementation decreases 12^{th} rib fat and decreases marbling score (Lean et al., 2014).

These supplements induce skeletal muscle cellular signaling by binding to G-protein coupled β-adrenoceptors (β-AR). This activates the cAMP and Protein Kinase A signaling pathway that results in CREB regulation of gene transcription (Mersmann, 1998). Downstream effects of these cellular signaling pathways are the physiological mechanisms underlying the production outcomes. β-AA have been reported to induce muscle hypertrophy by increasing the muscle fiber cross-sectional area and increasing muscle protein synthesis with no change in protein degradation (Bergen et al., 1989; Anderson et al., 1990; Hergenreder et al., 2017; Barnes et al., 2019). Feed efficiency is improved in part by improving the metabolic function of skeletal muscle (Cadaret et al., 2017; Barnes et al., 2019).

The adrenergic system is typically associated with the stress response. Several studies have evaluated if β-AA alter physiological parameters associated with stress. In multiple instances, ZH supplemented cattle undergoing a stress challenge had decreased body temperatures relative to controls (Boyd et al., 2015; Buntyn et al., 2016). β-AA act as vasodilators (Dawes Matthew et al., 1997), so one mechanism of lower body temperature could be a greater ability of β-AA supplemented animals to dissipate heat (Buntyn et al., 2016). Additionally, in response to an endocrine challenge, ZH supplemented heifers also had lower cortisol and epinephrine levels in the blood relative to non-supplemented controls indicating a possible downregulation of the hypothalamic–pituitary–adrenal axis due to ZH supplementation (Buntyn et al., 2016). To further evaluate the impact of β-AA on the stress response, researchers evaluated transcriptome changes; cattle supplemented RAC had little change in the whole blood transcriptome with no signs of systemic inflammation, but genes involved in inflammatory pathways

were upregulated including *IFI35*, *TYROBP*, and *TP53INP1* (Burrack et al., 2020). A study of RAC supplementation in pigs also reported a transcriptional integrated stress response as well as pathways associated with muscle metabolism (Brown et al., 2018).

Since the catecholamines produced in response to heat stress and β-AA both activate β-AR, there are concerns about the use of β-AA during instances of other stress (Mersmann, 1998). The purpose of this study was to determine if β-AA supplementation has an additive effect on physiological parameters associated with heat stress. These data will help inform livestock production practices during environmental stress.

Materials and Methods

This study was approved by the Institutional Animal Care and Use Committee at the University of Nebraska-Lincoln, which is accredited by AAALAC International. Red Angus-based steers (260 ± 25 kg) were acclimated to individual tie stalls or pens for 5 days prior to initiation of the trial. Steers were housed in either the control thermal neutral (TN; THI=68; n=11) or heat stress (HS; THI=73-85; n=12) conditions and supplemented with ZH (8.38 mg/kg DM/d; n=12) mixed at 1% in soybean meal as a carrier or only soybean meal (No Supplement; NS; n=11) in a 2x2 factorial. Heat stressed steers were fed ad libitum. Thermal neutral steers were pair-fed based on the previous day feed intake as a percentage of body weight of the heat stressed steers. *Longissimus* dorsi samples were collected via biopsy at days 3 and 10. At the time of biopsy, 2-3 mL local anesthetic (2% Lidocaine HCl) was injected. Samples were collected through an approximately 2-inch incision made ~20 cm cranial of the pelvic bone then flash-frozen.

The second biopsy was collected from the opposite loin muscle as the first. The cattle were harvested on day 21 at the University of Arizona Food Products and Safety Laboratory. A third sample of *longissimus dorsi* was collected and flash frozen following evisceration and skinning.

RNA from the *longissimus dorsi* muscle was isolated with the RNeasy Fibrous Tissue Mini Kit (Qiagen) following the manufacturer protocol. Quality of RNA was evaluated using an Agilent Bioanalyzer 2100 (Santa Clara, CA, USA). Muscle samples with RIN ≥ 6.7 (N=65) were sequenced using 100 bp, 3' Tag-Seq reads at the Genomic Sequencing and Analysis Facility at the University of Texas at Austin to a targeted minimum depth of 5 million reads per sample. Reads were trimmed using TrimGalore and HTStream to set minimum read quality at 20 and minimum output read length at 35. Transcripts were quantified with STAR as annotated in Bos_taurus.ARS-UCD1.2.99 (Dobin et al., 2013).

Differential expression (DE) analyses were performed with DESeq2 (Love et al., 2014) using a significance threshold False Discovery Rate of 0.05. Loci with 20 or more counts observed across all samples were kept for analysis. The model design included supplement, environment, and their interaction. Individual genes with an adjusted *P*-value< 0.05 were considered DE. In order to identify outlier samples, a variance stabilizing transformation was conducted on the normalized count matrix then a heatmap was utilized to visualize the correlation of gene expression for each pairwise combination among samples (Kolde, 2012). An average correlation of 0.75 or lower was considered the outlier cutoff. Pathway analysis (Qiagen) was conducted on all loci with a raw $P<0.05$. Pathways with $P<0.01$ were considered significant.

Results

The RNA had a mean RIN score of 9.08 ± 0.79. The average read depth was 5,924,851 ± 955,188 reads per sample with 90.36% ± 0.04% uniquely mapped reads. There were 19,131 genes in the muscle data that had at least one read. After quality control and removal of lowly expressed loci 6,769 genes remained for analysis.

Four outlier samples were identified. They were highly correlated with one other (>0.9) but less correlated with the rest of the samples (<0.75). Statistical evaluation of genes related to fiber type (*MYH1, MYH2,* and *MYH7)* indicated that the outlier samples (representing animals in each treatment group at day 10 except the ZH, thermoneutral group) had significantly (P_{adj}<0.001) lower expression for these genes than the rest of the samples. This potentially indicates a difference in muscle fiber type due to accidental sampling of an adjacent muscle. Following outlier removal, there was a minimum of 3 and an average of 5.08 animals per treatment and time combination in the muscle data set (Table 1).

In the muscle samples, 40 genes were differentially expressed (DE) due to supplement at day 10 and 6 genes were DE due to environment at day 21 (Table 2). There was little overlap of significant (P_{raw}<0.05) genes across time points due to either environment or supplement (Figure 1 and 2). Ingenuity pathway analysis identified 113 significant pathways in the muscle samples across all days and effects (Table 3). The interaction between supplement and environment had 24 significant pathways across time

points. Heat stress resulted in the predicted dysregulation of 23 pathways in muscle. β-AA supplementation resulted in 66 significant pathways.

Discussion

This study provides some of the first evidence that heat stress and β-AA supplementation in cattle do not work additively to alter stress pathways and instead demonstrates that β-AA may mediate some of the impacts of stress in the skeletal muscle of beef cattle. Based on our stringent FDR cutoff and analysis, few loci were individually differentially expressed. Pathway exploration, however, provided insight into the mechanistic effects of the treatments. Muscle responded to both heat stress and β-AA supplementation, but the responses showed little overlap between tissues, and expectedly changed with time. The change over time is likely due in part to metabolic adaptation to heat stress or desensitization of β-AR due to chronic stimulation (Lohse et al., 1990). These data contribute to the growing body of work in livestock species demonstrating that β-AA supplementation acts to moderate some physiological and transcriptomic responses to heat stress.

Heat Stress Alters Cellular Metabolism

Acute heat stress causes oxidative stress in oxidative skeletal muscle. In both pigs and broilers, reactive oxygen species production is increased in skeletal muscle following the inception of heat stress, indicating oxidative stress in the muscle (Ganesan et al.,

2017; Wang et al., 2019). A mechanism for increased ROS production is enhanced substrate oxidation in the mitochondria (Mujahid et al., 2005; Mujahid et al., 2007). This mechanism could be present in the steers of this study because oxidative phosphorylation, mitochondrial dysfunction, and fatty acid oxidation pathways are predicted to be dysregulated at day 3.

Adaptative mechanisms are activated in skeletal muscle to slow heat stress induced oxidative damage. One of the mechanisms by which cells adapt to heat stress is HIF-1 signaling. In this study, Hypoxia Inducible Factor 1 Subunit Alpha (*HIF1A)* was upregulated in the heat stressed steer skeletal muscle at day 21. Upregulation of *HIF1A* has also been reported in heat stressed gilts (Sanz Ferdez et al., 2015) and barrows (Y. Hao et al., 2016). This subunit is rapidly degraded during homeostasis but there is increased accumulation of this protein in response to hypoxia, heat stress, cytokines, ROS, and other stressors (Ely et al., 2014). During this cellular stress the alpha subunit binds to the constitutively expressed HIF1-β subunit to form the HIF-1 transcription factor that is responsible for regulation of target genes (Lundby et al., 2009). There are multiple potential causes of HIF-1 activation in the skeletal muscle of heat stressed animals in this study. During heat stress, sufficient oxygen is delivered to the muscle from blood (Montilla et al., 2014). Our group previously reported that lambs undergoing chronic heat stress were hyperoxic, with higher blood oxygen partial pressure than that of thermoneutral controls (Swanson et al., 2020). Yet, Montilla et al. (2014) proposed that during heat stress there is an impairment of the oxygen binding capacity of myoglobin-bound iron leading to cellular hypoxia and an increased abundance of *HIF1A* (Montilla et al., 2014). Increases in ROS production and cytokines can also activate *HIF1A*. Prior

work by our group has reported increased plasma levels of the inflammatory cytokine TNFα in heat stressed lambs (Swanson et al., 2020).

HIF-1 activation leads to a variety of downstream changes that aid in acclimation to heat stress. A proposed downstream effect in heat stressed skeletal muscle is switching metabolism toward glycolysis by downregulating mitochondrial oxygen consumption (Papandreou et al., 2006; Baumgard and Rhoads, 2013). Our data did not indicate changes in glycolysis due to heat stress, but the oxidative phosphorylation, mitochondrial dysfunction, and fatty acid oxidation pathways dysregulated at day 3 due to heat stress were not predicted to be dysregulated at the other collection time points. Another downstream effect is upregulation of vascular endothelial growth factor (VEGF) to increase oxygen delivery to tissues (Ely et al., 2014). The VEGF signaling pathway was upregulated in the skeletal muscle of heat stressed steers at day 21 in this study, downregulated in muscle due to ZH supplementation at day 10, and unchanged due to the interaction between heat stress and ZH. All of these downstream changes indicate that HIF-1 activation led to cellular adaptation to heat stress in the skeletal muscle of steers in our study. Our data also provide evidence of acclimation to heat stress over time due to a decreased number of significant genes (P_{raw}<0.05) due to environment across time points with day 3 having the highest number of significant genes and day 21 having the fewest.

β-AA mediated the oxidative stress response and downstream adaptive changes. Sirtuin signaling was upregulated in the skeletal muscle of ZH supplemented steers at day 21. Sirtuins are a family of proteins that play a role in maintenance of homeostasis by regulating cellular metabolism; they have been implicated in the cellular stress response (Ye et al., 2016). Multiple sirtuin genes are inhibitors of *HIF1A* indicating that increased

sirtuin function could be one mechanism by which β-AA mediate the heat stress response (Nakagawa and Guarente, 2011). Our group previously reported that bovine satellite cells treated with β-AA have a more efficient response to the stress of an ATP-depleted environment than control cells attributed to increased mitochondrial capacity (Sieck et al., 2020). Our group has also reported increases in glucose oxidation rates in the muscle strips of lambs and rats supplemented ZH that was independent of insulin activity and glucose uptake (Cadaret et al., 2017; Barnes et al., 2019). These data indicate that β-AA induced improvements in metabolic efficiency may be another mechanism by which steers in the heat stress and β-AA treatment group displayed fewer signs of an oxidative stress response and downstream adaptive changes than their control diet counterparts. Further evidence that β-AA increase metabolic efficiency is in the upregulation of *EEF1AKMT1* in the skeletal muscle of β-AA supplemented steers at day 10. This gene was also upregulated in the ceca of broilers with a low feed conversion ratio indicating that it plays a role in feed efficiency (Shah et al., 2019). The interaction between β-AA, sirtuins, and heat stress on cellular oxygen levels and consumption warrants further investigation to more fully understand how β-AA mediate oxidative stress.

β-AA Influence Muscle Growth and Metabolism

The mechanism by which β-AA supplementation induces muscle hypertrophy is not fully understood. Previous work by our group indicated that one way ZH induces muscle hypertrophy is by increasing fiber cross-sectional area (Barnes et al., 2019). Alternatively, RAC may induce muscle hypertrophy by increasing protein synthesis rates

(Bergen et al., 1989; Adeola et al., 1992). The genetic regulation of these outcomes has not been elucidated. One plausible mechanism for this outcome was reported in our data. *OAZ1* was downregulated in the skeletal muscle of β-AA supplemented animals at day 10. This gene is an inhibitor of ornithine decarboxylase (ODC), the rate limiting step of polyamaline synthesis (Lee and MacLean, 2011). Increased polyamaline levels are associated with increased β-AA induced skeletal muscle hypertrophy (Cepero et al., 1998). In skeletal muscle at day 10, β-AA supplementation also resulted in downregulation of *TENM4,* a genetic marker of myoblast quiescence (Pietrosemoli et al., 2017). However, previous studies have indicated that β-AA induced muscle hypertrophy is likely not due to increased muscle nuclei density (Gonzalez et al., 2008; Hergenreder et al., 2017). Therefore, it is likely that additional genes are involved in myoblast differentiation and proliferation in the skeletal muscle of β-AA supplemented animals.

The timing of β-AA induction of muscle hypertrophy is also not fully understood. β-AR become desensitized due to chronic stimulation (Lohse et al., 1990). Due to an increased desensitization over time, the maximal protein accretion response due to β-AA supplementation is reported 7 to 10 days after supplementation was initiated in pigs, with the response decreasing to about zero within six weeks (Mills, 2002). There was evidence of receptor desensitization in our data due to a decrease (P_{raw}<0.05) in the number of genes transcribed across time points.

During β-adrenergic cell signaling the second messenger cAMP activates protein kinase A (PKA) to activate or repress target proteins (Mersmann, 1998). Some of these target proteins are members of the Rho family of GTPases. Eight pathways involving these GTPases were dysregulated in skeletal muscle of the ZH supplemented steers at

days 10 and 21. One subfamily of these GTPases is RhoA (Bryan et al., 2005). Previous studies report that RhoA is involved in muscle hypertrophy, contraction, and myogenesis (Bryan et al., 2005; Møller et al., 2019). However, the role of the Rho family GTPases in β-AA induced cell signaling is unclear in our data due to variation in the directionality of the significant pathways and minimal evidence of altered downstream signaling outcomes.

Our study provides evidence that β-AA supplementation does not exacerbate the muscle transcriptome response to heat stress. Instead, supplementation mitigated the oxidative stress response due to heat stress in skeletal muscle. Optimizing cattle efficiency and upholding high standards of animal well-being are priorities of the beef industry. These data indicate that the use of β-AA is crucial to meeting these standards. Further, increasing our understanding of the molecular mechanisms of heat stress can lead to the development of novel mitigation strategies.

Table 1. Number of samples per treatment combination after outlier removal

Treatment	**Day 3 Muscle**	**Day 10 Muscle**	**Day 21 Muscle**
Termal Neutral, Control Diet	6	4	5
Heat Stress, Control Diet	5	5	6
Termal Neutral, Zilpaterol	5	3	6
Heat Stress, Zilpaterol	6	4	6

Table 2. Differentially Expressed Loci

Effect	Day	Gene ID	Log Fold Change	P_{adj}
Supplement	10	*MBNL1*	1.989	0.002
		TCP1	-3.251	0.002
		LOC104974460	-2.724	0.004
		CLVS1	-2.278	0.007
		RPL9	-6.232	0.008
		EEF1AKMT1	-3.570	0.008
		LOC112443469	-4.383	0.018
		LOC112446352	-3.028	0.018
		KATNB1	-3.386	0.019
		LOC112448166	-3.340	0.022
		LOC112442208	-2.515	0.023
		MIR133C	2.98	0.023
		MYL2	2.289	0.023
		TENM4	-4.672	0.023
		GRHL2	-1.829	0.028
		CTNS	-1.8	0.029
		LOC112446717	-2.16	0.029
		PRAP1	-2.758	0.029
		LOC101908535	-1.701	0.032
		NREP	1.29	0.032
		CDH23	-2.068	0.032
		CCDC189	-1.710	0.033
		LENG9	-1.605	0.033
		LOC104973551	-2.560	0.033
		MAPK15	-2.423	0.033
		NAT9	-1.075	0.033
		SMIM33	-2.1464	0.033
		IMPDH1	-4.734	0.039
		LOC101905571	-2.753	0.04
		OAZ1	-2.150	0.041
		LOC100848246	-1.921	0.042
		LOC112445512	4.613	0.042
		MAP3K15	0.653	0.042
		ZNF280B	-3.277	0.042
		CHRNA2	-2.032	0.043
		DNAH7	-1.935	0.044

		LOC104975561	-3.299	0.044
		MIA3	-1.403	0.044
		LOC112446351	-2.206	0.047
		CNOT11	-2.363	0.049
Environment	21	*HIF1A*	1.012	<0.001
		LOC101903734	0.847	0.002
		PDZD9	0.884	0.002
		HNRNPU	0.549	0.029
		MTUS1	0.751	0.029
		TMCO6	0.322	0.029

Figure 1. Differentially Expressed (P_{adj}<0.05) Genes Due to Environment Across Sample Collection Days

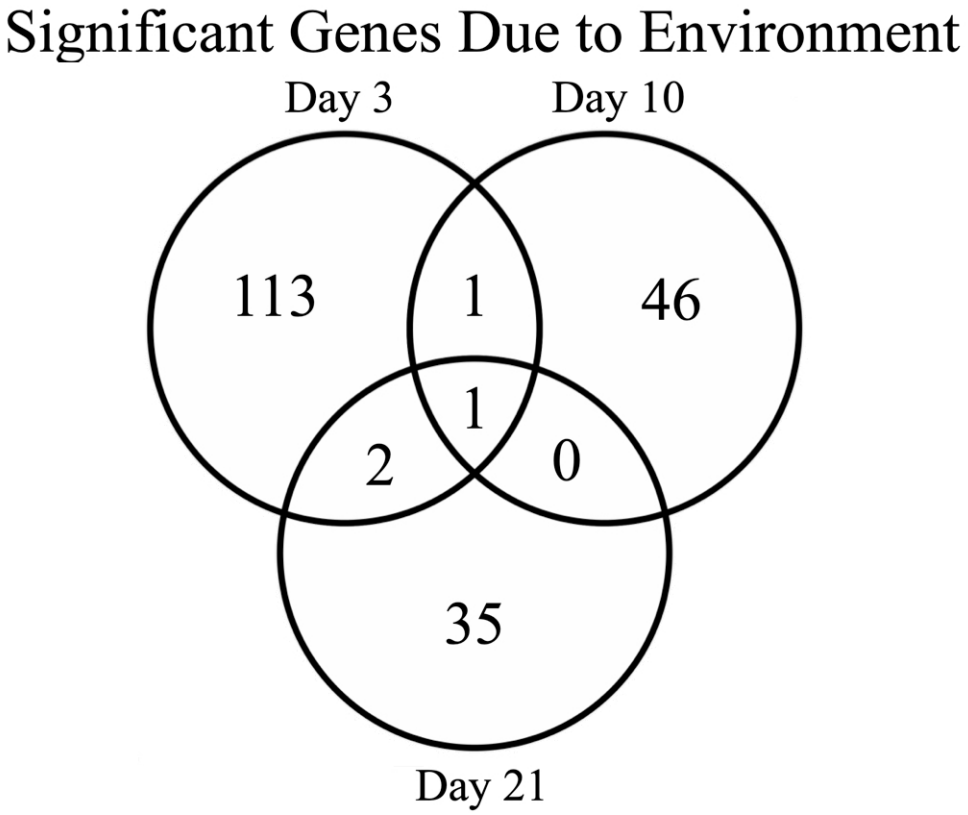

Figure 2. Differentially Expressed (P_{adj}<0.05) Genes Due to Supplement Across Sample Collection Days

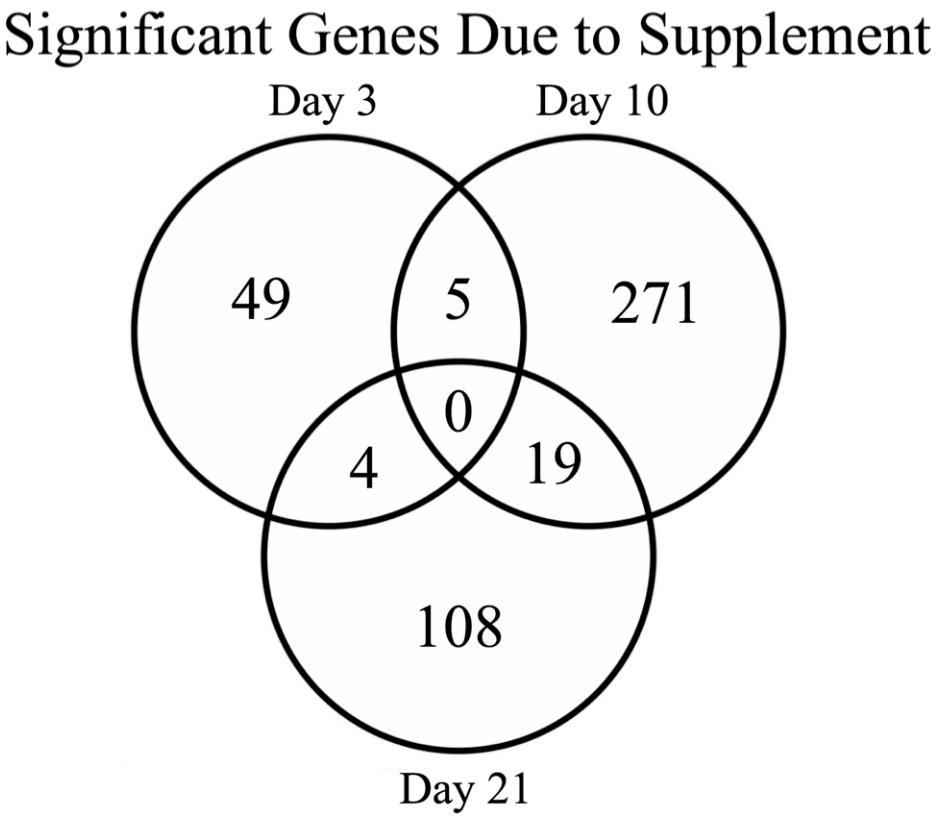

Table 3. Pathway Analysis

Effect	Day	Ingenuity Canonical Pathway	*P*-value	z-score
Interaction	3	mTOR Signaling	0.005	
		Circadian Rhythm Signaling	0.005	
		Cell Cycle Regulation by BTG Family Proteins	0.007	
		Role of IL-17F in Allergic Inflammatory Airway Diseases	0.009	
	10	Ferroptosis Signaling Pathway	<0.001	0
		p38 MAPK Signaling	0.003	
		Glutamine Degradation I	0.005	
		Acetate Conversion to Acetyl-CoA	0.010	
	21	Cardiac β-adrenergic Signaling	<0.001	0
		Role of CHK Proteins in Cell Cycle Checkpoint Control	0.001	
		BEX2 Signaling Pathway	0.003	
		Protein Kinase A Signaling	0.003	
		Apelin Adipocyte Signaling Pathway	0.003	
		TR/RXR Activation	0.003	
		Regulation of the Epithelial-Mesenchymal Transition Pathway	0.005	
		ERK/MAPK Signaling	0.006	-2
		Calcium Signaling	0.006	
		Estrogen Receptor Signaling	0.007	-0.447
		Telomerase Signaling	0.007	
		AMPK Signaling	0.007	
		Cell Cycle Regulation by BTG Family Proteins	0.008	
		cAMP-mediated signaling	0.009	
		HGF Signaling	0.009	
		RhoA Signaling	0.010	
Environment	3	Oxidative Phosphorylation	0.001	0
		β-linolenate Biosynthesis II (Animals)	0.002	
		Mitochondrial Dysfunction	0.006	
		Fatty Acid β-oxidation I	0.008	
	10	Colorectal Cancer Metastasis Signaling	0.001	1
		Cholecystokinin/Gastrin-mediated Signaling	0.001	

Environment	10	iNOS Signaling	0.003	
		HMGB1 Signaling	0.003	
		CXCR4 Signaling	0.003	
		EGF Signaling	0.004	
		Production of Nitric Oxide and Reactive Oxygen Species in Macrophages	0.004	
		GDNF Family Ligand-Receptor Interactions	0.008	
		Huntington's Disease Signaling	0.009	
		Cardiac Hypertrophy Signaling	0.009	
	21	Molecular Mechanisms of Cancer	0.002	
		Calcium Signaling	0.002	
		Endocannabinoid Cancer Inhibition Pathway	0.003	-1
		Colorectal Cancer Metastasis Signaling	0.005	0.447
		Glioblastoma Multiforme Signaling	0.005	
		BMP signaling pathway	0.006	
		VEGF Signaling	0.009	
		ILK Signaling	0.009	1
		Regulation of the Epithelial-Mesenchymal Transition Pathway	0.009	
Supplement	10	Calcium Signaling	<0.001	0
		Signaling by Rho Family GTPases	<0.001	-1.604
		Semaphorin Neuronal Repulsive Signaling Pathway	<0.001	1.155
		Tight Junction Signaling	<0.001	
		ILK Signaling	<0.001	0.577
		RhoA Signaling	<0.001	-1
		Epithelial Adherens Junction Signaling	<0.001	
		Apelin Cardiomyocyte Signaling Pathway	<0.001	-1
		Hepatic Fibrosis / Hepatic Stellate Cell Activation	<0.001	
		Actin Cytoskeleton Signaling	<0.001	0
		PAK Signaling	<0.001	-0.707
		Gα12/13 Signaling	<0.001	-0.333
		Cellular Effects of Sildenafil (Viagra)	<0.001	
		Regulation of Actin-based Motility by Rho	<0.001	-0.378
		AMPK Signaling	<0.001	-1
		Agranulocyte Adhesion and Diapedesis	<0.001	
		Cardiac Hypertrophy Signaling	<0.001	-0.905
		Uracil Degradation II (Reductive)	0.001	
		Thymine Degradation	0.001	
		RhoGDI Signaling	0.001	0.707
		HGF Signaling	0.001	-1.342

Supplement	10	Clathrin-mediated Endocytosis Signaling	0.001	
		CXCR4 Signaling	0.002	-0.707
		VEGF Signaling	0.002	-1.342
		Germ Cell-Sertoli Cell Junction Signaling	0.002	
		Integrin Signaling	0.002	-1.667
		PTEN Signaling	0.002	2.449
		Cardiomyocyte Differentiation via BMP Receptors	0.002	
		Cdc42 Signaling	0.002	0.816
		IGF-1 Signaling	0.002	-2.236
		FAK Signaling	0.002	
		Hereditary Breast Cancer Signaling	0.002	
		Triacylglycerol Biosynthesis	0.003	-1
		Cardiac β-adrenergic Signaling	0.003	0.447
		Production of Nitric Oxide and Reactive Oxygen Species in Macrophages	0.003	-1.414
		Estrogen Receptor Signaling	0.004	-1.508
		Gluconeogenesis I	0.005	
		Glycolysis I	0.005	
		VEGF Family Ligand-Receptor Interactions	0.005	
		ERK/MAPK Signaling	0.005	-0.378
		EGF Signaling	0.006	-2
		Axonal Guidance Signaling	0.006	
		Thrombin Signaling	0.006	
		RANK Signaling in Osteoclasts	0.006	-1.342
		CTLA4 Signaling in Cytotoxic T Lymphocytes	0.006	
		Cancer Drug Resistance by Drug Efflux	0.007	
		IL-12 Signaling and Production in Macrophages	0.008	
		IL-2 Signaling	0.008	
		MSP-RON Signaling in Cancer Cells Pathway	0.009	-1.633
		Salvage Pathways of Pyrimidine Ribonucleotides	0.009	1.342
		Nitric Oxide Signaling in the Cardiovascular System	0.010	-0.447
	21	Sirtuin Signaling Pathway	<0.001	1.342
		Tight Junction Signaling	<0.001	
		ILK Signaling	<0.001	0
		TR/RXR Activation	0.001	
		Actin Cytoskeleton Signaling	0.001	1.633
		IGF-1 Signaling	0.002	

Supplement	21	RhoA Signaling	0.003	1
		Granzyme A Signaling	0.004	
		Cellular Effects of Sildenafil (Viagra)	0.004	
		Estrogen Receptor Signaling	0.006	-0.816
		GDNF Family Ligand-Receptor Interactions	0.006	
		Cardiac Hypertrophy Signaling	0.007	0.447
		Epithelial Adherens Junction Signaling	0.007	
		Glioblastoma Multiforme Signaling	0.009	
		L-DOPA Degradation	0.010	

CHAPTER 3: β-ADRENERGIC AGONISTS ALTER OXIDATIVE PHOSPHORYLATION IN SKELETAL MUSCLE CELLS

Introduction

Beta-adrenergic agonists are FDA-approved supplements utilized in pigs and cattle to improve growth performance, carcass weight, and longissimus muscle area (Lean et al., 2014). Previous studies within our group have focused on understanding molecular changes in skeletal muscle due to beta-adrenergic agonist (β-AA) supplementation. This work has shown that β-AA supplementation increases glucose oxidation in muscle from thermoneutral and heat-stressed lambs and in rat skeletal muscle stimulated with ZH. These effects were independent of insulin signaling and glucose uptake, indicating alterations in cellular efficiency (Cadaret et al., 2017; Barnes et al., 2019). Skeletal muscle transcriptomics of lambs supplemented ZH revealed upregulation of mitochondrial solute carrier *SLC25A25* (Kubik et al., 2018). *SLC25A25* is a Ca^{2+} sensitive ATP-$Mg^{2+/}$Pi inner mitochondrial membrane solute transporter. Due to the role of the mitochondria in metabolism, the objective of this study was to understand how β-AA affect mitochondrial function of skeletal muscle stem (i.e., satellite) cells isolated from cattle, pigs, and sheep. We hypothesized that β-AA would improve the efficiency and ATP production capacity of muscle satellite cells by modifying mitochondrial function.

Materials and Methods

Isolation of Satellite Cells

This study was approved by the IACUC at the University of Nebraska-Lincoln, which is accredited by AAALAC International. Skeletal muscle was collected from cattle and pigs at the USDA-inspected abattoir at the University of Nebraska-Lincoln. Additionally, pig and sheep skeletal muscle was collected via surgery from control animals in other studies at the University of Nebraska-Lincoln. Collected muscle was placed in cold PBS on ice. Connective tissue, fat, and membranes were dissected away from the muscle and the muscle was minced. Minced tissue (approximately 5 mL) was divided into 50 mL conical tubes and washed in 30 mL cold PBS. The tubes were centrifuged at 1500 x g for 5 min and supernatant was poured off into the sink. Protease from *Streptomyces griseus* (Sigma-Aldrich, St. Louis, MO) buffer was prepared with 0.0375 g Protease and 30 mL PBS per 50 mL conical tube. The protease buffer was stirred on a hot plate at 37ºC until the solution was nearly clear. Then it was filtered using a 0.22 μm filter (Millipore Sigma) into a sterile bottle. Cells were digested in the protease buffer by placing the 50 mL conical tubes in a 37ºC water bath for 1 hr and vigorously shaking for approximately 10 sec every 15 min. Tubes were centrifuged at 1500 x g for 5 min and supernatant was poured off. Myoblasts were separated from tissue via serial centrifugation. 22.5 mL of 37°C 1X PBS was added to each conical tube. Tubes were vigorously shaken for ~10 sec then centrifuged at 500 x g for 10 min. Supernatant was collected. Pellets were resuspended in 18.5 mL of 37°C 1X PBS, tubes were vigorously shaken for ~10 sec, then centrifuged at 500 x g for 8 min. Supernatant was collected.

Pellets were again resuspended in 12.5 mL of 37°C 1X PBS. Tubes were vigorously shaken for ~10 sec and then were centrifuged at 500 x g for 1 min. Supernatant was collected and filtered with 100 µm filter conical tubes (Millipore Sigma). Filtered fluid was centrifuged at 1500 x g for 5 min. Supernatant was aspirated off and pelleted satellite cells were suspended in 15 mL media (90% DMEM (Thermo-Fisher Scientific, Waltham, MA) and 10% Fetal Bovine Serum (Atlanta Biologicals, Flowery Branch, GA) and incubated on Cell Culture Microplates (Agilent Technologies) at 37°C and 5% CO_2 for 2 hr to remove fibroblasts. The media and non-adhered myoblast mixture was collected into a 50 mL conical tube. Plates were washed with an additional 10 mL of PBS and the PBS was added to the conical tube. Tubes were centrifuged at 1500 x g for 5 min. Supernatant was aspirated off and pelleted cells were resuspended in 15 mL growth media (78.5% DMEM, 20% Fetal Bovine Serum, 1% AbAm (Thermo-Fisher Scientific, Waltham, MA), and 0.5% gentamycin (Thermo-Fisher Scientific, Waltham, MA) per 15 cm culture plate. Cells were seeded onto Poly-L-Lysine and Fibronectin coated cell culture plates and incubated at 37°C and 5% CO_2.

Satellite cells were detached from plates for splitting or freezing using 10 mL Accutase (Innovative Cell Technologies, Inc., San Diego, CA). The cells suspended in Accutase were collected into a 50 mL conical tube then plates were washed with an additional 10 mL of 37°C 1X PBS; the PBS was added to the conical tube. Conical tubes were centrifuged at 1500 x g for 5 min. Supernatant was aspirated off and pelleted cells were resuspended in 37°C 1X PBS and counted using a hemocytometer. Conical tubes were again centrifuged at 1500 x g for 5 min and supernatant was aspirated off. For splitting, pelleted cells were resuspended in growth media and seeded onto coated cell

culture plates. For freezing, pelleted cells were resuspended in freezing media (74.76% DMEM, 19.05% Fetal Bovine Serum, 4.76% DMSO (Thermo-Fisher Scientific, Waltham, MA), 0.95% AbAm, 0.48% gentamycin). 500 µL of cells suspended in freezing media was pipetted into each 2.0 mL cryo tube and placed in a freezing container and stored at -80°C. After at least 24 hours, cryo tubes were moved to liquid nitrogen for long term storage.

Seahorse Assay

Satellite cells were detached and counted as described above. Based on seeding density optimization trials, pelleted cattle cells were suspended in growth media at a concentration of 100,000 cells per 100 µL. Pelleted sheep and pig cells were suspended in growth media at a concentration of 125,000 cells per 100 µL. 100 µL of media with suspended cells was added to 20 of the wells in a Poly-L-Lysine and Fibronectin coated Cell Culture Microplate (Agilent, Santa Clara, CA) incubated at 37°C and 5% CO_2 for 10 min. Each Microplate had 4 blank wells filled with 250 µL growth media. After incubation, 150 µL growth media was added to each well with cells and plates were incubated at 37°C and 5% CO_2 overnight. The assay was performed using a Seahorse XFe24 Analyzer (Agilent, Santa Clara, CA) following the manufacturer's protocol (Seahorse XF Cell Mito Stress Test Kit User Guide, 2019) with the following modifications. 50 mL of Seahorse DMEM Media was supplemented with 500 µL Sodium Pyruvate (100 mM), 500 µL Glutamine (200 mM) and 500 µL Glucose (2 M). An FCCP

titration was performed (0 μM to 2 μM). FCCP, Oligomycin, and Rotenone were prepared by combining 300 μL stock solution and 2,700 μL of supplemented Seahorse DMEM Medium. 55 μL of Oligomycin was added to port A, 65 μL of FCCP was added to port B and 70 μL of rotenone was added to port C. 50 μL of the β-AA treatment was added to port D. For each cell line species, a concentration trail for Zilpaterol (ZH; 0.05 μM to 0.2 μM) and Ractopamine (RAC; 1 μM to 4 μM) was performed. For final data collection, ZH was used at a concentration of 0.1 μM and RAC at a concentration of 2 μM for all species. Each drug was diluted in supplemented Seahorse DMEM medium; supplemented medium without β-AA was injected as the control treatment.

Following the Seahorse run, media was aspirated from wells. 75 μL of RIPA buffer (Thermo-Fisher Scientific, Waltham, MA) was added to each well and pipetted vigorously. Protein concentration for each well was determined using either a Pierce BCA Protein Assay Kit or a Pierce Coomassie Plus (Bradford) Assay Kit (Thermo Fisher Scientific, Waltham, MA) following the manufacturer's protocol. Oxygen Consumption Rate (OCR) data were normalized to the estimated protein concentration of each well in the Seahorse Wave desktop software.

Well and individual measurement outliers were excluded as previously described (Yépez et al., 2018). Since intracellular flux studies result in considerable inter-plate variation (Yépez et al., 2018), the OCR for each well was standardized based on fold change relative to the average baseline OCR for that well (time points 2-6). Then, standardized technical replicates for every cell line x treatment x time point were averaged. Oxygen Consumption Rate (OCR) metrics were calculated based on the

manufacturer's user guide (Seahorse XF Stress Test Report Generator User Guide, 2016) with the following modifications due to data standardization (Figure 1, Table 1). Basal OCR was calculated by subtracting the Non-Mitochondrial OCR from 1. ATP Production was calculated by subtracting the minimum rate after Oligomycin injection (time point 7-9) from 1. The effect of β-AA treatment was analyzed by ANOVA with the GLIMMIX procedure in SAS (SAS Institute). Cell isolate was the experimental unit (n=15).

Results

Considerable variation was observed in time point 1 readings, attributed to variation in machine calibration time. Therefore, time point 1 was excluded from evaluation in all plates and was not used in the calculation baseline OCR used in normalization. There was no significant change in OCR in response to acute injection for species (P= 0.6564), β-AA injection (P= 0.8901) or the interaction between the two (P= 0.7565). Therefore, average baseline OCR was calculated using the reads before (time point 2 and 3) and after (time point 4-6) the injection of β-AA treatments to allow for a greater number of data points and a more accurate baseline OCR for normalization.

Incubation of cells with either ZH or RAC increased maximal respiration (P= 0.046) and spare respiratory capacity (P= 0.0352) in bovine satellite cells (Figure 2). No difference was observed between ZH and RAC (P>0.05). In porcine and ovine satellite cells, maximal respiration and spare respiratory capacity did not differ between β-AA treated cells and controls (Figure 2 and 3). No differences were observed among treatments or animals for basal respiration, ATP-linked respiration, proton leak, or non-

mitochondrial respiration in any of the species due to β-AA treatment (P>0.05; Figure 2, 3 and 4).

Discussion

In this study we found that both RAC and ZH enhance spare respiratory capacity and maximum respiration of bovine muscle stem cells but resulted in no metabolic changes in porcine or ovine cells. This demonstrates that β-AA supplements improve the efficiency of bovine myogenic cells by favorably modifying mitochondrial function. The RAC and ZH-treated cells are better equipped to respond to the stress of an ATP-depleted environment than control cells due to their increased mitochondrial capacity. We postulate that this leads to more efficient utilization of available substrates and more efficient energy production in the muscle of β-AA supplemented cattle. This study also demonstrates mitochondrial efficiency is one plausible mechanism underlying the differing physiological responses to β-AA across species.

One mechanism by which β-AA improve cattle production outcomes is by altering glucose metabolism and mitochondrial function. Previous studies by our group have reported increased glucose oxidation in primary skeletal muscle isolated from lambs that were supplemented ZH and in primary rat muscle stimulated with ZH in vitro (Cadaret et al., 2017; Barnes et al., 2019). These effects were independents of insulin signaling and glucose uptake, indicating alterations in cellular efficiency. These data led us to investigate the role mitochondria play in cellular efficiency changes. Our results indicate that β-AA increased maximum, but not basal respiration rate in bovine cells. We

postulate that this is due to the increased intracellular availability of substrates to be oxidized in these cells. Uncoupling agents like FCCP can mimic the physiological energy demand typical of a muscle during exercise (Adhihetty et al., 2003). This uncoupling causes the respiratory chain to function at its maximum possible rate to re-establish the ion gradient. Rapid oxidation of substrates like sugars, fats, or amino acids is required to complete this response (Seahorse XF Cell Mito Stress Test Kit User Guide, 2019). Bovine myoblasts treated with β-AA demonstrated an increased capacity to oxidize substrates than their control media counterparts.

Spare respiratory capacity, the difference between basal and uncoupler-stimulated respiration, reflects the cells' ability to respond to increased energy demands (Divakaruni et al., 2014). Cells with a greater spare respiratory capacity typically have decreased demands at resting state and increased mitochondrial biogenesis at different stages of the cell cycle (Divakaruni et al., 2014). Mitochondrial biogenesis in muscle is characterized by an increase in mitochondrial density in cells and increased enzyme activity within cells (Adhihetty et al., 2003). Since cells in this study were treated acutely with β-AA before measurement, it is unlikely that the response observed in bovine myoblasts was due to increased mitochondria number. Instead, it is plausible that β-AA treatment resulted in increased enzymatic activity in the oxidative phosphorylation pathway. An increase in enzymatic activity would result in more efficient ATP production in the cell, which could have implications in animal performance measures such as feed-to-gain ratios. Future experiments evaluating enzyme activity are warranted to evaluate the impact on animal performance and differences between species in cells treated with RAC and ZH.

The lack of an effect of β-AA on basal respiration rates in bovine, porcine, or ovine myoblasts leads us to believe that β-AA do not play a role in the electron transport chain of cells in a resting state. This substantiates our assertions regarding changes in glucose oxidation in β-AA treated cells. In a state of rest, cell mitochondria utilize a finite amount of substrate regardless of the amount available. Therefore, we would not anticipate a difference in basal mitochondrial function between treated and untreated cells. In addition to basal respiration, β-AA did not affect proton leak, non-mitochondrial respiration, or ATP-linked respiration, demonstrating no evidence of mitochondrial dysfunction, as would be suspected if proton leak was significant there was a negative alteration in ATP-synthase (Divakaruni et al., 2014; Yépez et al., 2018). This also assumes that cells had equal amounts of oxygen consumption by non-mitochondrial oxidases (Divakaruni et al., 2014).

Cattle, pigs, and sheep have differing changes in feed efficiency and muscle and fat deposition in response to β-AA supplementation at an organismal level, therefore species differences in the response to β-AA treatment at a cellular level are unsurprising (Mersmann, 1998). Species differences observed between cattle and pigs in this study were expected due to differences in the β-AR isoforms located on the cell surface. Cattle skeletal muscle has predominantly β_2-AR, but β_1-AR and a small portion of β_3-AR are also present (Sillence and Matthews, 1994). Alternatively, pig skeletal muscle primarily has the β_1-AR subtype with a smaller number of β_2-AR and an even smaller proportion of β_3-AR (McNeel and Mersmann, 1999). Species differences observed between cattle and lambs were more surprising. Lambs are often used as a physiological model for cattle because of similar metabolic and growth regulating systems (Barnes et al., 2019).

However, this study provided evidence of metabolism differences between the species. Receptor subtype abundance has not been explicitly studied in sheep but feeding trials resulted in a more robust response to β_2- than β_1-AA so similar to cattle, sheep skeletal muscles are presumed to have primarily the β_2-AR subtype (Lopez-Carlos et al., 2011). Therefore, alternative physiological mechanisms are likely underlying the species differences in mitochondrial function between cattle and sheep. Further studies are warranted to understand the differing effects of β-AA supplementation on cellular metabolism across species.

There are many possible sources of variation in mitochondrial function between animals within a species. A positive correlation between mitochondrial efficiency and feed efficiency has been reported in broilers, pigs, and beef cattle (Bottje and Carstens, 2009; Grubbs et al., 2013). Therefore, cells isolated from high feed efficiency or low feed efficiency animals would be expected to have differing mitochondrial function. Further, mitochondrial function varies across breeds of livestock. Differences were reported between Angus and Brahman cattle, potentially contributing to the heat tolerance differences between the breeds (Ramos et al., 2020). Our study did not take breed composition or feed efficiency into account before cell line isolation, which may contribute to variation within the species we evaluated. Evaluation of these variables in future studies could help characterize intra-species variation.

Our data indicate that both ZH and RAC increase maximal respiration and spare respiratory capacity relative to controls in bovine muscle stem cells. Thus β-AA treated bovine cells have indicated an increased ability to respond to cellular stresses and increased energy demands. This provides evidence that favorable modification of

mitochondrial capacity is one mechanism by which β-AA supplements increase metabolic and growth efficiency of skeletal muscle in livestock. However, a lack of significant change in mitochondrial function due to β-AA treatment in porcine and ovine cells indicates that additional physiological mechanisms contribute to β-AA improvement of feed efficiency in livestock animals.

Table 1. Mitochondrial function calculations based on OCR

Measure	**Calculation**
Non-mitochondrial respiration	Min OCR (time point 13-15)
Basal respiration	1 – Non-mt respiration
Maximal respiration	Max OCR (time point 10-12) – Non-mt respiration
Proton leak	Min OCR (time point 7-9) – Non-mt respiration
ATP-linked respiration	1 – Min OCR (time point 7-9)
Spare respiratory capacity	Maximal respiration – Basal respiration

Figure 1. Experimental design for Seahorse XF Cell Mitochondrial Stress Test

Oxygen Consumption Rate (y-axis) is measured at 15 time points (open circles) before and after the addition of β-AA (or no/control treatment) and three drugs. The expected response of the cell is shown, and measures of mitochondrial function illustrated (Seahorse XF Stress Test Report Generator User Guide, 2016).

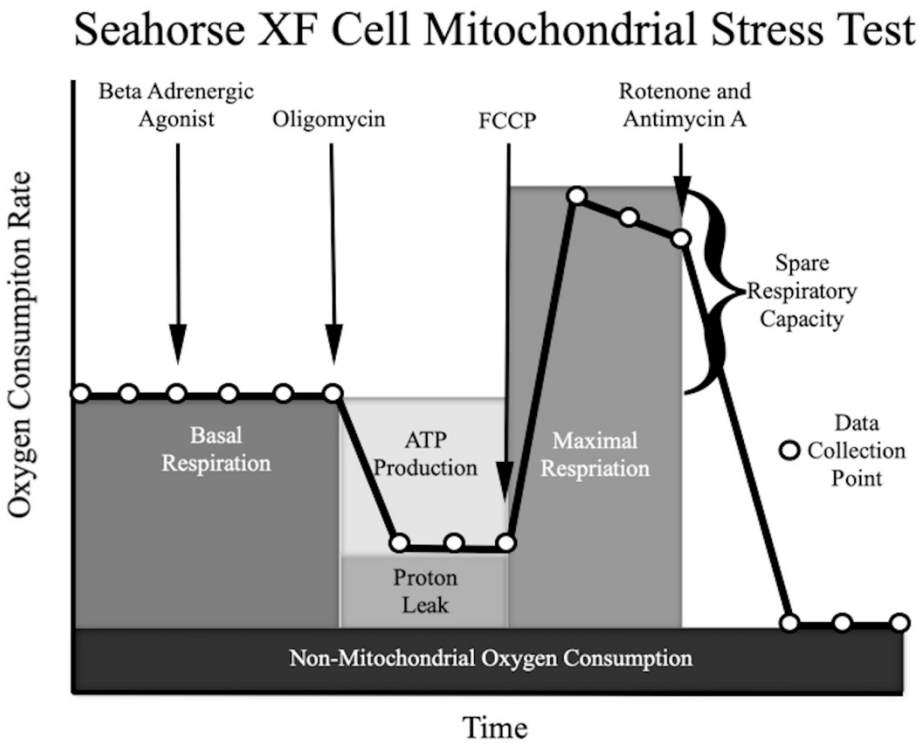

Figure 2. Bovine Measures of Mitochondrial Function

Least squared means (± std err) for each treatment across each measurement of mitochondrial function (OCR relative to baseline time points 2-6). * signifies a difference ($P<0.05$) relative to control (no treatment).

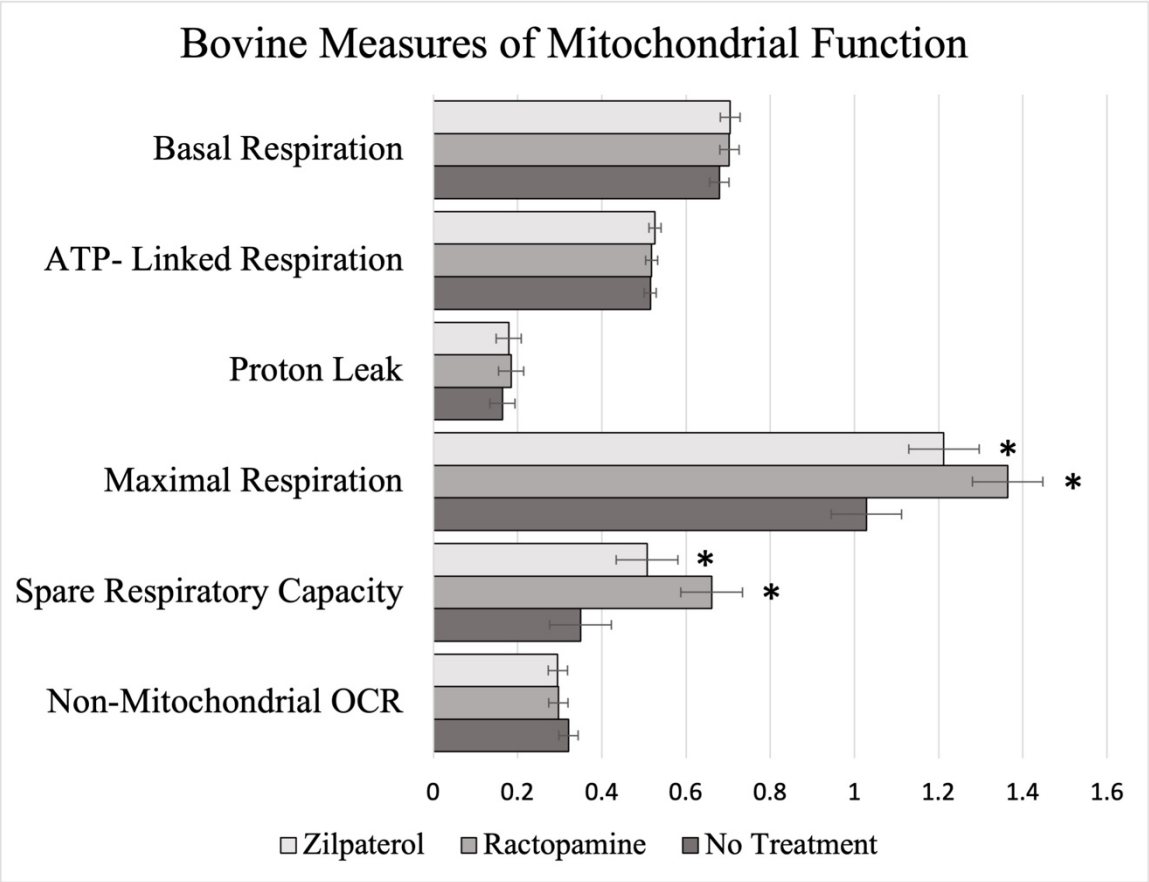

Figure 3. Ovine Measures of Mitochondrial Function

Least squared means (± std err) for each treatment across each measurement of mitochondrial function (OCR relative to baseline time points 2-6). No significant differences were measured.

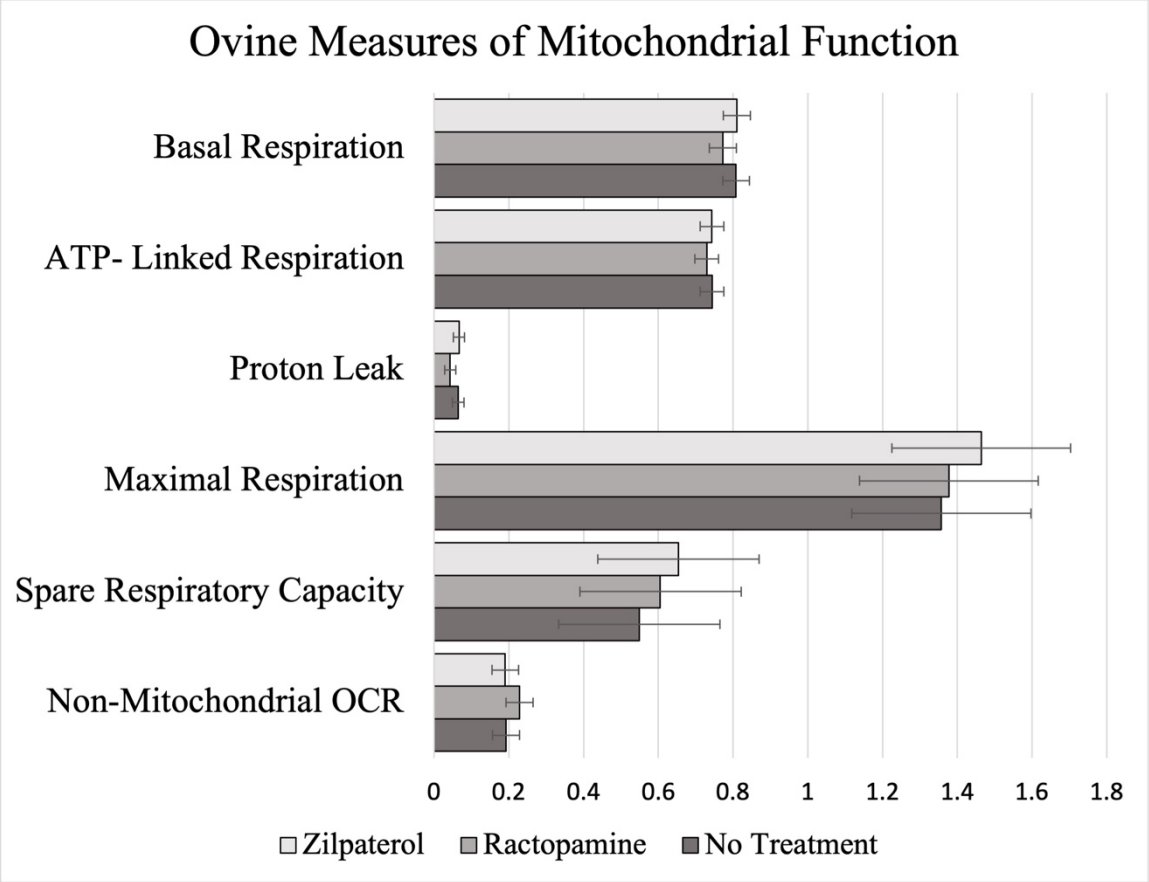

Figure 4. Porcine Measures of Mitochondrial Function

Least squared means (± std err) for each treatment across each measurement of mitochondrial function (OCR relative to baseline time points 2-6). No significant differences were measured.

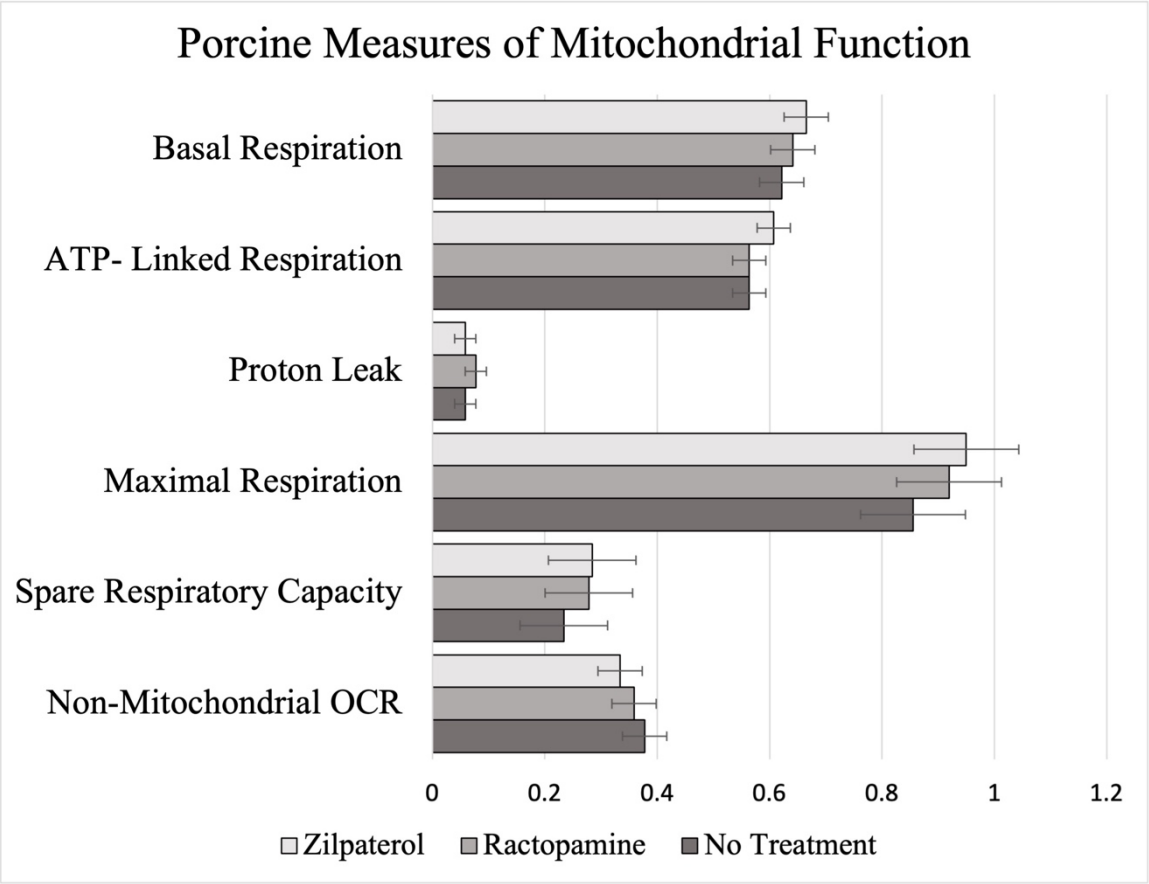

CHAPTER 4: MANDIBULOFACIAL DYSOSTOSIS ATTRIBUTED TO A RECESSIVE MUTATION OF *CYP26C1* IN HEREFORD CATTLE[1]

[1] Sieck, R. L., Fuller, A. M., Bedwell, P. S., Ward, J. A., Sanders, S. K., Xiang, S. H., Peng, S., Petersen, J. L. & Steffen, D. J. (2020). Mandibulofacial Dysostosis Attributed to a Recessive Mutation of *CYP26C1* in Hereford Cattle. *Genes*, *11*(11), 1246.

Introduction

Over 250 Mendelian traits in cattle are reported in the Online Mendelian Inheritance in Animals database (https://omia.org/home/). Often deleterious syndromes in cattle are attributed to variants inherited in an autosomal recessive manner (Ciepłoch et al., 2017). Due to this inheritance pattern, clinical signs of disease may not appear for many generations after the casual mutation originates. However, artificial selection in livestock and the commonplace use of artificial insemination and embryo transfer can expedite widespread proliferation of a deleterious variant. Once a deleterious defect is identified, prompt identification of carrier animals is necessary to prevent economic loss. The significant impact of a single deleterious variant in livestock can be exemplified by a recessively inherited mutation in *APAF1*, traced back to a Holstein bull born in 1962. The recessive genotype, detrimental to cow fertility, was estimated to have resulted in 525,000 abortions costing the industry $420 million (Adams et al., 2016).

In March and April of 2020, three herds reported a total of six purebred Hereford calves born with unusual defects of the face and jaw attributed to a condition we termed Mandibulofacial Dysostosis (MD). One of the reporting herds also noted a calf born with a similar phenotype in 2018. The calves were live born, of normal size, with an intact suckle reflex but weak suckling ability. Grossly, several calves appeared to have a widened upturned "smile," a variably shortened and/or asymmetric lower mandible, and unique, bilateral skin tags just caudal to the commissure of the lips. The three herds reporting MD cases were each in a different state (Iowa, Wyoming, Missouri) with typical summer grazing and winter feeding programs, making an environmental cause unlikely. Sires and dams of affected calves were consanguineous.

The similarity in the reported clinical description among the affected calves, the pedigree analysis, and description of similar phenotypes in children (Chen et al., 2018) and mice (Vieux-Rochas et al., 2007; Gitton et al., 2010) led to the hypothesis that a de novo, autosomal recessive mutation may be causative of this novel condition in Hereford cattle. Pathologic findings of Meckel's cartilage suggested that a mutation might exist that disrupts development of PA1, possibly through ET1 and DLX signaling. Expression of Dlx homeobox genes in the cranial neural crest cells (CNCC) of first pharyngeal arch (PA1) provides patterning information during jaw formation. Differentiation between the mandible and maxilla is driven by endolithin-1 (ET1) signaling in PA1 that activates Dlx5 and Dlx6 (Vieux-Rochas et al., 2007; Parada and Chai, 2015). The identification of a causative variant would allow breeders to identify carrier individuals to avoid production of affected calves and has the potential to yield novel information regarding the regulation of craniofacial development. To investigate this hypothesis, multiple

affected calves were obtained to establish a phenotypic characterization of the defect and case definition. DNA from these calves, family members, and herd mates was collected for whole-genome sequencing (WGS) to identify possible de novo variant(s) impacting mandibulofacial development in the affected calves.

Materials and Methods

Animals utilized in this study were sampled in compliance with approved University of Nebraska IACUC project ID number 1970: Diagnostic Investigation into Natural Animal Disease Events. Five affected calves, two heifers and three bulls, were received at the University of Nebraska-Lincoln Veterinary Diagnostic Center (UNL-VDC) for autopsy evaluation, four after euthanasia on the farm and one live, within 24 hours of birth. The live calf was evaluated for hearing and vision, and then euthanized by intravenous injection of pentobarbital sodium and phenytoin sodium (Euthosal, Virac AH, Inc.).

Sire and dam of all reported, affected calves as well as their extended pedigrees (records available through the American Hereford Association, https://hereford.org/) were evaluated to identify common ancestors. The herd of origin and date of birth was also noted.

Tissue samples (ear) were collected from the five affected calves received at the UNL-VDC. Semen or whole blood samples were obtained from parents of affected calves (as available) and initially from 7 other related individuals. All samples were stored at -20°C. DNA was isolated from blood samples using a Gentra Puregene Blood

Kit (Qiagen, Venlo, Netherlands) utilizing the following protocol. Blood tubes were centrifuged at 2,000 x g for 15 min at 4°C. 250 µL of buffy coat was combined with 900 µL red blood cell lysis solution, vortexed to mix, and then incubated at room temperature for 5 min. Samples were then centrifuged (13,000 x g for 2 min); the supernatant was discarded. 450 µL of red blood cell lysis solution was then added to the tube containing the pellet, vortexed to mix, and then incubated at room temperature for 5 min. Samples were again centrifuged (13,000 x g for 2 min). The supernatant was discarded and 900 µL cell lysis solution and 6 µL Proteinase K was added. The samples were vortexed, then incubated for 30 min at 35˚C. After cooling on ice to room temperature, 200 µL of protein precipitation solution was added, the samples were vortexed for 1 min, and then incubated on ice for 5 min. The tubes were centrifuged (13,000 x g for 2 min at room temperature). The supernatant was poured into a new tube containing 800 µL of 100% isopropanol and tubes were inverted 50 times to precipitate DNA followed by centrifugation at 8000 x g for 2 min. The supernatant was discarded, and tubes were drained on a clean paper towel for 1 min. 300 µL of 70 % ethanol was added and tubes were inverted to wash DNA and centrifuged (8000 x g for 1 min). The supernatant was again discarded, and tubes were drained for 10-15 min on a clean paper towel before the DNA was rehydrated in 100 µL of DNA hydration solution. Samples were incubated at room temperature overnight before storage at 4˚C.

DNA isolation from semen was also completed using the Gentra Puregene Blood Kit (Qiagen, Venlo, Netherlands) with modifications as previously described (Petersen et al., 2019). DNA quality and purity were evaluated with an Epoch Microplate Reader (BioTek, Winooski, VT, USA). Isolated DNA samples from 20 individuals underwent

KAPA library preparation and sequencing with 150-bp paired-end reads across one lane of an Illumina NovaSeq S4 at Admera Health (South Plainfield, NJ, USA). Adapters and poor-quality bases (minimum Phred score 20) were removed using Cutadapt (Martin, 2011) via the wrapper TrimGalore version 0.4 (https://github.com/Felix Krueger/TrimGalore). The sequences were mapped to the ARS-UCD1.2 reference genome using BWA–MEM (Li, 2013) and the output .sam files converted to .bam files and indexed using SAMtools (Li et al., 2009). Duplicate reads were marked using Picard (http://broad institute.git hub.io/picard). Variants were called across all individuals with a freebayes-parallel (https:// github.com/ekg/freebayes/blob/master/scripts/freebayes-parallel), and variants with a quality score lower than 30 were eliminated. Variant positions (e.g., intronic, exonic) were annotated using the ARS-UCD1.2 Annotation Release 106.

Filtering to identify candidate variants was completed utilizing VCFtools (https://vcftools.github.io). Some variants were further prioritized by evaluating their predicted impact on gene/protein function as annotated by the Ensembl Variant Effect Predictor (https://uswest.ensembl.org/info/docs/tools/vep/index.html) and SNPEff (Cingolani et al., 2012).

Sequence Read Archive data were obtained for animals mapped to the ARS-UCD1.2 and UMD3.1 reference genomes using a workflow based upon https://github.com/SichongP/SRA_variant_search. The NCBI Genome Remapping Service (https://www.ncbi.nlm.nih.gov/genome/tools/remap) was used to translate variant positions between genome builds. The pileup function from the sra-tools (https://github.com/ncbi/sra-tools, version 2.9.1) was used to generate pileup files at

candidate variant loci. Subsequent genotyping was carried for loci with at least 10 reads per locus.

For verification of the leading candidate SNP, 762 additional samples (semen, EDTA blood, or hair) were obtained. Of these samples, 289 were banked DNA samples from the American Hereford Association stored at Neogen GeneSeek (Lincoln, NE, USA), which were received in the form of isolated DNA. DNA was isolated from the blood and semen samples as described above. DNA from hair was isolated as previously described (Petersen et al., 2020).

One of three genotyping methods were employed for validation of the candidate variant. Kompetitive Allele Specific PCR genotyping was conducted using primers and probes designed with the KASP on Demand utility (LGC Genomics, Teddington, Middlesex, UK; S1 Table). All KASP reactions were performed in duplicate on a CFX384 Touch Real-Time PCR machine (Bio-Rad, Hercules, California) following the manufacturer's protocol. Non-template (negative) controls, 3 homozygous reference controls, 3 heterozygous controls, and 4 homozygous alternative controls were run on each plate. The fluorophores HEX and FAM labeled wildtype and variant probes, respectively. Results were visualized in the CFX Maestro Software (Bio-Rad Laboratories, Hercules, CA, USA).

Any sample failing to genotype in duplicate via KASP was genotyped by either Sanger sequencing or ddPCR. For ddPCR assays, primers to amplify a 136-bp fragment containing the candidate variant were designed in Primer3 (Untergasser et al., 2012) (S1 Table). PrimeTime, double-quenched (ZEN/IowaBlack FQ) competitive probes were constructed to distinguish between the wildtype (T) and variant (C) alleles, labeled with

HEX and FAM fluorophores, respectively (S1 Table). ddPCR reactions were performed using standard protocol on a QX200 ddPCR system (Bio-Rad Laboratories, Hercules, CA, USA). A non-template (negative) control was included as well as positive controls, which consisted of DNA from two affected calves, two obligate carriers, and two unaffected individuals. Samples of interest for allele quantification were run in duplicate or triplicate. The reaction included 1X ddPCR Supermix for Probes (no dUTP; Bio-Radlaboratories), 25 ng (10ng/µl) of template DNA, primers at 0.18 µM each, probes at 0.02 µM each, and molecular grade water to a final reaction volume of 22 µL. Reactions were converted into approximately 20,000 one-nanoliter droplets using the QX200 Droplet Generator. Thermocycling included 10 min of enzyme activation at 95°C and 39 cycles of denaturation (94°C, 30 sec) followed by annealing/extension (64°C, 1 min). Enzyme deactivation (98°C, 10 min) concluded the cycle. The plate was read in the QX100 Droplet Reader (Bio-Rad) and results were analyzed using QuantaSoft Software (Bio-Rad). Power to distinguish alleles was determined from the false-negative rate of the controls (e.g., power for detection of a variant allele =1−
(wildtype droplets/total positive droplets), when template representing only the variant allele was provided).

Sanger sequencing was performed for 6 different variants at ACGT, Inc. (Wheeling, IL, USA) after PCR with primers designed in Primer3 (Untergasser et al., 2012) (S1 Table). PCR reactions were performed using a FastStart kit (Sigma-Aldrich, St. Louis, MO, USA) and included 4.45 µL water, 0.25 µL MgCl, 1.2 µL 10X buffer with MgCl, 0.5 µL dNTP, 0.1 µL Taq, 0.75 µL of 20uM forward and reverse primer, and 4µL of 5ng/µL DNA template. Thermal cycling conditions consisted of 94°C for 4 min,

32 cycles of 94°C for 30 sec, annealing temperature (S1 Table) for 30 sec, 72°C for 45 sec, a final extension at 72°C for 10 min, then a 10°C hold. PCR product cleanup was performed using 0.75 μL ExoSAP-IT (Applied Biosystems) per 4 μL PCR product. Thermal cycling conditions consisted of a cycle at 37°C for 30 min, 80°C for 15 min and 15°C hold.

The cytochrome CYP26C1 (*Bos taurus*) structural model was generated based on the X-ray crystal structure of cyanobacterial CYP120A1 (Kühnel et al., 2008) (PDB: 2VE3) using sequence homology modeling program Modeller (Webb and Sali, 2016). Their protein sequences have a 31.4% identify and 46.8% similarity. The secondary structural predictions were conducted using an online Jnet program and the window size setup for 22 amino acids based on the structure of the α-helix segment from 179 to 200 amino acids. Conservation of the amino acid altered by the most promising candidate SNP was also evaluated across multiple species using Multialign (http://multalin.toulouse.inra.fr/multalin/).

Whole-genome sequence data generated for this project are available on the NCBI SRA (BioProject ID: PRJNA663547). Sanger sequencing data representing each *CYP26C1* genotype have been deposited in GenBank (Accessions: MW123048 and MW123049). Novel candidate variants have been deposited in the European Variation Archive (EVA) (Project ID: PRJEB40605).

Results

Pathologic Characteristics of Affected Calves

Autopsy evaluation of five affected calves, three bulls and two heifers, took place at the UNL-VDC. The calves weighed between 32 and 41 kg. Unique and consistent hallmarks of the condition included bilateral skin tags 2-10 cm caudal to the commissure of the lips (Figure 1A, 1B). The tags were 0.5-2.0 cm long with a central dermal core that attached through a short, 1 cm dermal band to cartilage (Figure 1C). This cartilage extends to its origin at the zygomatic process of the temporal bone (Figure 1D). The cartilage, from its origin extended cranially for 3-5 cm and was encased in bone. The boney processes were 1.5-2.0 cm wide, 1.0 cm thick and separated from underlying bones of the face by a 0.5 cm gap. A short 1.0 cm dorsal lateral protrusion of bone at the origin of the boney process was also present. The bone-wrapped Meckel's cartilage was bilateral and consistent in each affected calf. When the bone was fractured during autopsy, a perfectly round 0.35 mm diameter tube of cartilage freely separated in the center of the bone (Figure 1E). Several affected calves had additional skin tags near or several centimeters below the external acoustic meatus not associated with cartilage or bone (Figure 1A, 1B). Additional coexisting facial deformities included megastomia in three, camplyognathia of the mandible in two, campylognathia involving mandible and maxilla in one, and brachgnathia inferior in three calves (Table 1). A single calf had a cleft palate. The calves with maxillary campylognathia also had asymmetry of the orbits with one located approximately 3 cm caudal to the other. All calves had hypoplasia of the masseter and temporalis muscles and pinnae that were low set and drooped.

Histologic evaluation of the boney process originating from the temporal bone revealed a cartilage (Meckel's) core sandwiched between plates of bone (Figure 1F). The

bone and cartilage were surrounded by thick fibrous periosteum. No evidence of endochondral ossification is noted with this cartilage. Sections of eye, kidney, liver, brain, adrenal, spleen, skeletal muscle, thymus, intestine, and lymph node appear normal. The skin tag had a thick dermal core with redundant collagenous stroma and most sections included normal adnexa and sinus hairs.

After disclosure of the MD defect to the breed association membership, three additional affected calves were reported, with the phenotype of two confirmed via digital image evaluation, and one by evaluation at the UNL-VDC. All affected calves had the presumed founder in their pedigree (Figure 2).

Whole Genome Sequencing

Whole genome sequence data, averaging 13.0X coverage (range 10.8 to 15.5; standard deviation 1.32) of 20 individuals (3 affected calves, parents of the sentinel cases (N=6), parents of other affected calves (N=4; including that of the 2018 calf) and 7 related individuals (S1 Figure) was filtered to identify variants that were homozygous for the alternative allele in all affected calves, in a heterozygous state in all obligate carriers (parents of affected calves), and either heterozygous or homozygous for the reference allele in the related individuals. This filtering resulted 143 variants matching the hypothesized recessive mode of inheritance; all but 17 had RefSNP (rs) identifiers. 134 of the candidate variants were located between 10.3 and 15.9 Mb on chromosome 26 (S2 Table). Evaluating the variants homozygous in the calves without regard to the genotype

of other individuals identified an extended region of homozygosity among cases that also included this region of chromosome 26.

Additional evaluation was performed using WGS data from 101 animals sequenced for other projects in the lab (including 6 purebred Hereford and 8 Hereford-crosses), from 1,577 cattle sequenced previously as part of the 1000 bull genomes project (Daetwyler et al., 2014), and 128 other Herefords provided by the American Hereford Association. These data resulted in the elimination of 141 of the 149 candidate variants as one or more of the additional animals were homozygous for the alternative allele. Of the remaining 8 variants, one was a missense variant in Exon 3 of *CYP26C1* (Chr26 g. 14404993T>C), one SNP was in the 5' untranslated region of *TBC1D12* (Chr26 g. 15898152C>T), and the other 5 were intronic or intergenic (Table 2). The missense variant was the only variant with a predicted impact (SIFT score = 0, deleterious).

Candidate Variant Filtering

A query of the Sequence Read Archive yielded results for 3191 cattle at one or more of the 8 variants queried. These samples represent the Hereford, Angus, Red Angus, and Simmental breeds and others. At 6 of the remaining 8 variants queried, all cattle in the SRA search were homozygous reference, providing no information from which to further filter them from the data set. Two variants were eliminated as possible causative variants due to their presence in other breeds as MD appears to be unique to the Hereford and associated with one specific bloodline. At chr26 g.10713132G>A, 6 of 1018 samples were heterozygous for the alternative allele (alt. frequency: 0.006). These 6

samples were of breeds including Romagnola, Simmental, and Original Braunvieh. Seven out of 1083 samples were heterozygous and 1 homozygous for the alternative allele at chr26 g.10794674G>A (alt. frequency: 0.0083). These 8 samples were also Romagnola, Simmental, and Original Braunvieh.

Sanger sequencing was performed on the 6 remaining candidate variants in one of the additional affected calves, 3 additional parents of these affected calves, the presumed founder animal, the presumed sire of the founder animal, and 25 animals with the presumed founder bull in both their maternal and paternal pedigree. These data ruled out 4 of the 6 remaining candidate variants due to identification of animals that genotyped homozygous for the alternative allele but did not display the MD phenotype or due to the MD affected calf not genotyping as homozygous for the alternative allele. Of the two variants that could not be ruled out with additional data, due to its predicted function the missense variant in *CYP26C1* was the primary candidate of interest and focused upon for further analyses.

CYP26C1 Variant Genotyping

782 Hereford cattle were genotyped for the *CYP26C1* SNP including the WGS animals (N = 20), other cattle from two of the reporting herds (N = 623), the suspect founder, two additional affected calves, and parents of those affected calves (N = 4) (Table 3). Of these 782, 624 were homozygous for the reference allele, 153 heterozygous, and the 5 affected calves homozygous for the variant allele. Within these Herefords genotyped, 106 had the presumed founder bull in both the sire and dam side of their

pedigree, 327 had the presumed founder bull in one side of their pedigree, and 348 animals were not descendants of the presumed founder (Table 3). Notably, the suspect founder genotyped heterozygous, all additional affected calves from which DNA was available were homozygous for the alternative allele, and parents of the additional affected calves were heterozygous (DNA on one dam not available). Twelve animals were calves of both a sire and dam that were confirmed carriers of the *CYP26C1* variant allele; of these, 2 were homozygous for the reference allele, 5 heterozygous, and 5 homozygous for the variant allele (all affected with the described MD phenotype).

In total, 3371 genotypes for the *CYP26C1* g.14404993T>C locus were examined (Table 4). With the exception of 17 of the 20 cattle sequenced for this study, the variant was not identified in any WGS-derived genotype.

Power to distinguish between wildtype and variant alleles by ddPCR was 0.999 and 0.998, respectively. An average of 9999.9 droplets (st dev = 1599.8) were read per sample, with each run in 2 or more replicates. The germ line variant allele frequency of the maternal grandsire and great grandsire of the suspect founder did not exceed that of wildtype controls (S3 Table), refuting a hypothesized mosaic origin of the variant in either bull.

Predicted Impact on Protein Function

Alignment of the amino acid sequence of *CYP26C1* indicated that the residue altered (p. L188P) was conserved across *Bos taurus, Ovis aries, Sus scrofa, Equus caballus, Homo sapiens, Mus musculus, Danio rerio, Xenopus tropicalis,* and *Canis lupus*

familiaris (Figure 3). Structural modeling demonstrated the mutation site of L188P is located at the α-helix segment from 179 to 200 amino acids. This is not within the heme active site at which the substrate binds such as the all-trans-retinoic acid (atRA). Secondary structural predictions, however, indicate that the α-helix will be broken if the leucine (L) is substituted with proline (P) at the position 188 (Figure 4).

Discussion

In this investigation, MD of Hereford calves was associated with a missense mutation in *CYP26C1*. MD is detrimental to the viability of affected animals due to an impaired ability to nurse. The identification of this associated and putatively causative marker provides breeders the ability to test for carriers to avoid mating decisions that may produce an affected calf. Animals with the presumed founder on both sides of their pedigree originated from over 40 different breeders showing the widespread implications of MD within the Hereford breed. Further, the implication of *CYP26C1* provides insight into the role of this gene in the regulation of RA during the development of craniofacial structures.

Facial structures including the mandible, maxillary musculature, and some structures of the inner ear and hindbrain are derived embryonically from CNCC that migrate from the neural tube to the PA1. This region of the embryo is the most rostral of the anteroposteriorally segmented structures present in early development (McGeady et al., 2017). Expression of Dlx homeobox genes in the CNCC of PA1 provides patterning information that results in specification of the mandibular and maxillary arches (Gitton et

al., 2010; Parada and Chai, 2015). Differentiation between the mandible and maxilla is driven by ET1 signaling in PA1 that activates *Dlx5* and *Dlx6* resulting in formation of Meckel's cartilage in the mandibular, but not the maxillary prominence (Vieux-Rochas et al., 2007; Parada and Chai, 2015); Meckel's cartilage, a transient cartilaginous plate, serves as a scaffold during formation and elongation of the intramembranous mandible bone (Granstrom et al., 1988).

Migration and proliferation of CNCC is guided by gradients of signals including fibroblast growth factor, retinoic acid, and Wnt (Parada and Chai, 2015; Schilling et al., 2016). Retinoic acid (RA) plays a critical role in PA1 development because it acts as a repressor of ET1 (Vieux-Rochas et al., 2007). Excess RA disrupts ET1 signaling acting on the Dlx genes. Therefore, excess exposure of PA1 to RA during a critical developmental period results in teratogenesis of the mandible, specifically altering development of the Meckel's cartilage. Similar effects were observed in *Dlx5/Dlx6* and in ET1 receptor mutant mice (Ruest et al., 2004), supporting the importance of RA in the development of mandibular structures. Dysregulation of the RA gradient has the most severe effect on craniofacial morphology at 9 to 14 somites (Vieux-Rochas et al., 2007); during this period, migrating cranial neural crest cells reach PA1 (Serbedzija et al., 1992). Nine-somite mouse embryos treated with excess RA had malformed Meckel's cartilage (Vieux-Rochas et al., 2007; Gitton et al., 2010) while the cartilage developed normally when treated outside of this developmental time point (Vieux-Rochas et al., 2007). For cattle, this critical developmental window would fall around day 21 or 22 of gestation (Noden, 1966; Thomsen, 2003).

The concentration of RA in the developing embryo is regulated in a tissue-specific manner by opposing actions of synthesizing (Raldh) and metabolizing (Cyp26) enzymes (Tahayato et al., 2003). The *CYP26C1* gene and its counterparts, *CYP26A1* and *CYP26B1,* oxidize RA into inactive polar metabolites enabling the maintenance of the RA gradient across the pharyngeal arches (Williams and Bohnsack, 2019). Studies elucidating the expression patterns of *CYP26C1* show it is expressed in PA1 during the critical time point for RA teratogenesis. For example, using whole-mount in situ hybridization, Tahayato et al. (2003) showed expression of this gene in PA1 of mouse embryos from E8.0 – E9.5 (approximately 1 to 30 somites).

There are multiple lines of evidence that alteration of *CYP26C1* function results in developmental abnormalities. Knockdown of *CYP26C1* in zebrafish embryos resulted in increased RA levels associated with atypical development of the pharyngeal arches and otic vesicles (Montalbano et al., 2016). *CYP26A1* and *CYP26C1* null mice also had deficient development of PA1 and PA2 and altered migration of cranial neural crest cells (Uehara et al., 2007). The studies indicate that normal function of *CYP26C1* is critical to avoid morphological changes in craniofacial structures.

We postulate that the association of the *CYP26C1* missense mutation and abnormal development of the jaw in MD calves can be attributed to the loss of catalytic activity resulting in reduced ability of the enzyme to metabolize RA. The affected amino acid is not located in the canonical heme thiolate-binding motif (FxxGxxxCxG) that is characteristic of the P450 family of proteins to which CYP26C1 belongs (Slavotinek et al., 2013). However, proline is a helix breaker and our model supports that the L188P mutation results in a structural change to the α-helix (Kim and Kang, 1999). This chance

may affect the active site structure for substrate binding and a subsequent loss of function impairing metabolism of RA. Further, this amino acid residue is conserved across species. Both the protein model and the evolutionary maintenance of the amino acid serve as further evidence the *CYP26C1* L188P mutation is deleterious to protein function.

Reports of craniofacial deformities in cattle commonly include cleft palate or more severe dysplasias (Oryan et al., 2011; Sartelet et al., 2014; Agerholm et al., 2017). A recent report from India identified a calf with a pathology similar to MD (Kumar et al.). This, however, is the first comprehensive report of the novel MD phenotype in Herefords, which we believe is attributed to a de novo mutation in the sire common to the pedigree of all calves. Semen from the suspect founder genotyped heterozygous for the *CYP26C1* SNP with no evidence of germ-line mosaicism as studied by ddPCR. Semen of this bulls' sire and both maternal grandsires were homozygous for the reference allele at the *CYP26C1* SNP, also confirmed by ddPCR. DNA was not available from the (deceased) mother of the presumed founder bull, therefore origination of the variant in the maternal lineage of our presumed founder cannot be excluded. Even with the possibility of maternal origin, the bull common to all pedigrees of affected calves has been the primary perpetuator of the variant resulting in the manifestation of this phenotype. To this point, no carrier animals have been identified that do not have the presumed founder in their pedigree. Further, both the presumed founder and his sire genotyped as heterozygous for the only other remaining candidate variant (Chr26 g. 15898152C>T). If this variant was causative, we would expect to have identified MD cases in decedents of the sire of the suspect founder without a pedigree connection to the

suspect founder himself; that has not been the case, contributing to the body of evidence that the variant in *CYP26C1* is causative of this condition.

Several human conditions exhibit similar pathologies to MD calves. One hallmark of MD in all affected calves is the presence of skin tags located along the fusion site of the maxillary and mandibular prominences. Strikingly similar skin tags are observed in Hemifacial Microsomia patients (Chen et al., 2018). Focal facial dermal dysplasia, Type IV, is also characterized by skin lesions and polyps on the buccal mucosa located at the same fusion site (Slavotinek et al., 2013). Notably, both human syndromes are attributed to similar developmental pathways as implicated in MD. Focal facial dermal dysplasia is caused by loss of function mutations in *CYP26C1* and one model of causation for hemifacial microsomia includes altered migration, differentiation and proliferation of cranial neural crest cells in PA1 (Chen et al., 2018).

A condition also termed Mandibulofacial Dysostosis is described in human literature as a heterogeneous anatomic group of disorders; the described condition in Hereford cattle is not analogous to human MD. The human MD condition more broadly affects chondrocyte and osteoblast differentiation with dysostosis most apparent in, but not limited to, the face (Ahmed et al., 2016). Implicated mutations in *EFTUD2* in human MD are unrelated to CNCC migration and differentiation (Lines et al., 2012; Wieczorek, 2013). Further, the normal facial features of humans and bovines differ dramatically with cattle being more dolichocephalic; thus, we do not anticipate homologous anatomic outcomes due to disruptions in branchial arch related processes.

A defining and novel characteristic of Hereford MD is the retention of Meckel's cartilage past early development and shortening of the mandible. No human conditions

have been described exhibiting this precise pathology, but similarities in a group of human syndromes termed “retinoic acid embryopathies” exist. These embryopathies have been described to result in micrognathia, cleft palate, and microtia or anotia (Lammer et al., 1985). One of the affected MD calves exhibited cleft palate as observed in human retinoic acid embryopathies. Additionally, Hemifacial Microsomia patients manifest hypoplasia of the mandible due to decreased blood supply to the Meckel’s cartilage (Wiszniak et al., 2015).

Finally, calves exhibited a range of severity in phenotype in the truncation of the lower jaw, presence of additional skin tags, and in one case the additional feature of a cleft palate. Variation in human syndromes affecting craniofacial development is also common. For example, the severity of Hemifacial Microsomia can range from moderate hypoplasia to complete absence of a portion of the jaw with other neural and muscular symptoms (Gitton et al., 2010). Similarly, in a set of infants with malformations due to RA exposure, 14% exhibited cleft palate (Lammer et al., 1985). We propose that variation in phenotype of the MD calves may be attributed to intrinsic variability in RA availability during development.

Supplement Table 1 (S1 Table). Genotyping primers and probes

Genotyping Method	**Variant Location**	**Forward Primer**	**Reverse Primer**	**Fragment Length (bp)**	**Annealing Temp (C)**
Sanger Sequencing	Chr7: 15413	TGCATGGTCA GCCAAGTA	AATTGAAGGC CATGATAACG	488	60
Sanger Sequencing	Chr26: 10588399	CGATTCGCTA AGGCTCATTC	AAGCCCTAGC ACCCTAAAGC	582	56
Sanger Sequencing	Chr26: 10616433	GCCCAGAGCT TTTAGCTTCC	TGGGGTTCTG GAATGGATTA	546	58
Sanger Sequencing	Chr26: 10982292	TCCAATACTTT GGCCACCTC	GCAGCCACTT TTTGAAGGAG	534	60
Sanger Sequencing	Chr26: 14404993	CGAGAGCAAA ACCCAACACA	TCAAAGGGAA AGTCTGGGGC	454	62
Sanger Sequencing	Chr26: 15898152	AACCTGACCC TGAGGGAACT	ATAATTCCAG CACCCCATGA	520	62
Genotyping Method	**Variant Location**	**Forward Primer**	**Reverse Primer**	**Wildtype Probe (HEX)**	**Variant Probe (FAM)**
ddPCR	Chr26: 14404993	GCCGGTCGCT GTCTATG	GAAGAGGTTC TCCACGAACT G	CTAAAGCGCTCA CCTTCCGCATGG	TAAAGCGCCC ACCTTCCGCAT
Genotyping Method	**Variant Location**	**Primer Allele T (reference)**	**Primer Allele C (variant)**	**Common Primer**	
KASP	Chr26: 14404993	GCGGCCATGC GGAAGGTGA	CGGCCATGCG GAAGGTGG	GTCGCTGTCTAT GAGGCCGCTA	

Supplement Figure 1 (S1 Figure). Pedigree of all Whole Genome Sequenced Animals

Filled shapes represent affected calves, half-shaded shapes are carriers, and open shapes represent the reference genotype. Animals for which DNA was not available at the time of Whole Genome Sequencing are shown in grey; all others (black) were genotyped for the *CYP26C1* variant. Males are denotated as rectangles, females are ovals, the presumed founder bull is a diamond.

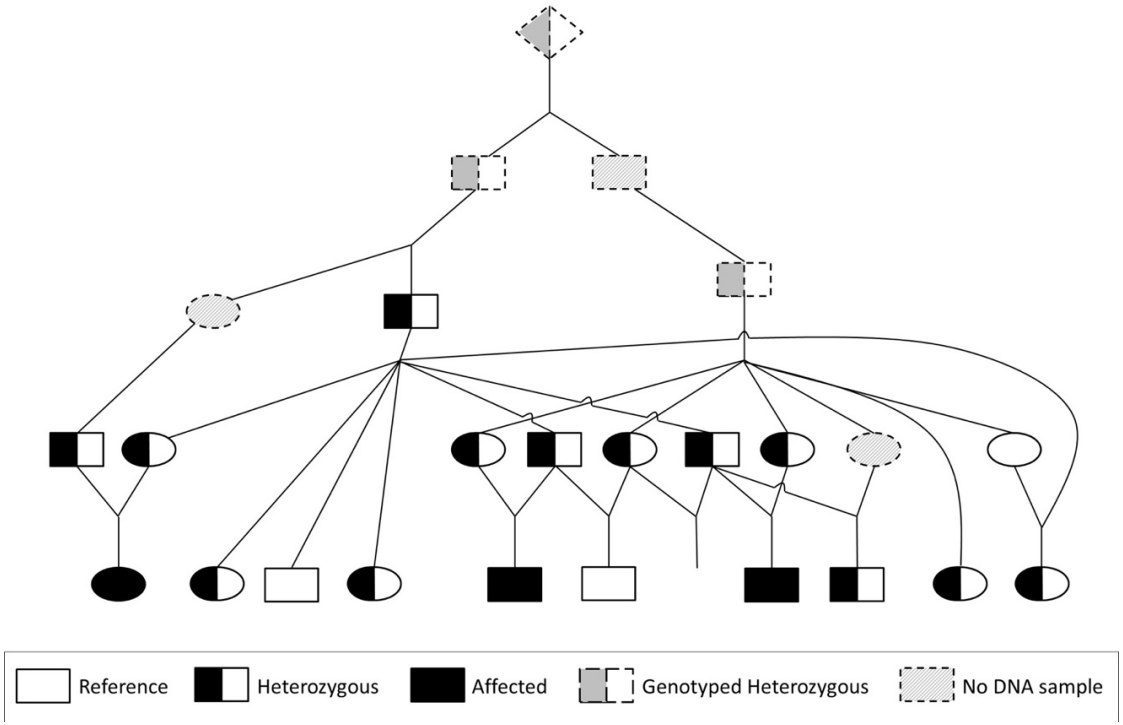

Figure 1. Images of calves affected with Mandibulofacial Dysostosis (MD)

A. An MD calf with megastomia. Skin tags are visible ventral to the eye and at the base of the ear. Brachygnathia is also evident, and a slight facial bulge is seen dorsal and caudal to the skin tag. B. An MD calf with skin tags; one is caudal to commissure of the lips and one is ventral to the base of the ear near the caudal ramus of the mandible. C. Exposure of the abnormal bone in an MD calf with the skin tag intact at the right margin. D. The skull of an MD calf showing the exposed bone fractured during autopsy and demonstrating origin of this abnormal bone just above the temporal mandibular joint. E. An image of the fractured boney prominence in an MD calf exposed the retained Meckel's cartilage within the bony prominence. F. Histology evaluation of the Meckel's cartilage core from an MD calf surrounded by bone and separated by fibrous tissue.

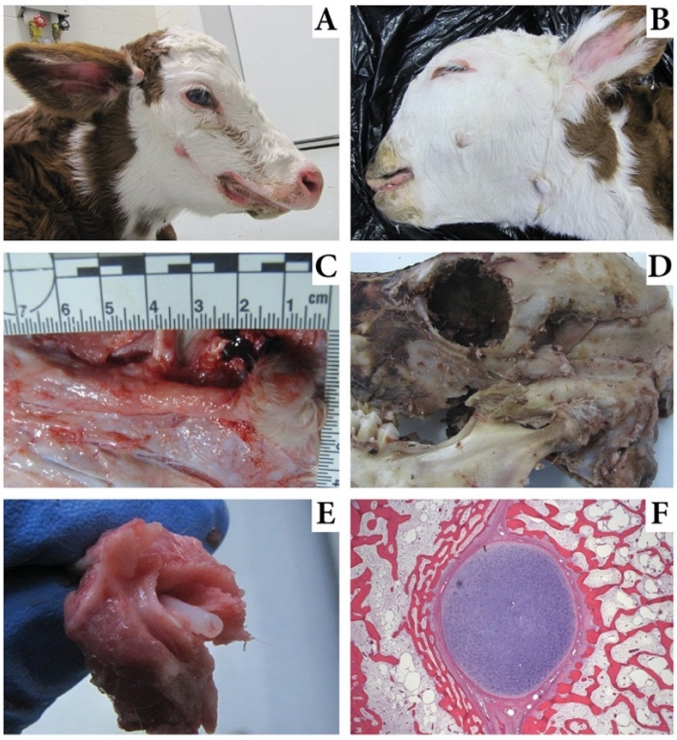

Table 1. Pathologic Characteristics of Mandibulofacial Dysostosis Calves

Given is a list of the hallmark and variable characteristics observed in MD calves and indicators of which animals displayed each. The dash (-) indicates an attribute that was not examined.

Pathologic Description	**Calf 1**	**Calf 2**	**Calf 3**	**Calf 4**	**Calf 5**
Bilateral bone-wrapped Meckel's cartilage	yes	yes	yes	yes	yes
Bilateral skin tags 2-10 centimeters caudal to the commissure of the lips	yes	yes	yes	yes	yes
Skin tags near or below the external acoustic meatus	-	yes	yes	yes	yes
Pinnae that were low set and/or drooped	yes	yes	yes	yes	yes
Hypoplasia of the masseter and temporalis muscles	yes	yes	yes	yes	yes
Megastomia	yes	yes	no	no	yes
Brachgnathia inferior	yes	no	no	yes	yes
Campylognathia involving mandible and maxilla	no	no	yes	no	yes
Asymmetry of the orbits	no	no	yes	no	yes
Cleft palate	yes	no	no	no	no
Sex of Calf	female	male	male	male	female

Figure 2. Pedigree of Affected Animals

Pedigree of affected calves that were included in the WGS dataset and additional affected calves reported after disclosure of the MD defect to the breed association membership (N=10; males=rectangles, females=ovals, unknown sex=triangles). Filled shapes represent affected calves, half-shaded shapes are carriers, and open shapes represent the reference genotype. Animals for which DNA was not available are shown in grey; all others (black) were genotyped for the *CYP26C1* variant.

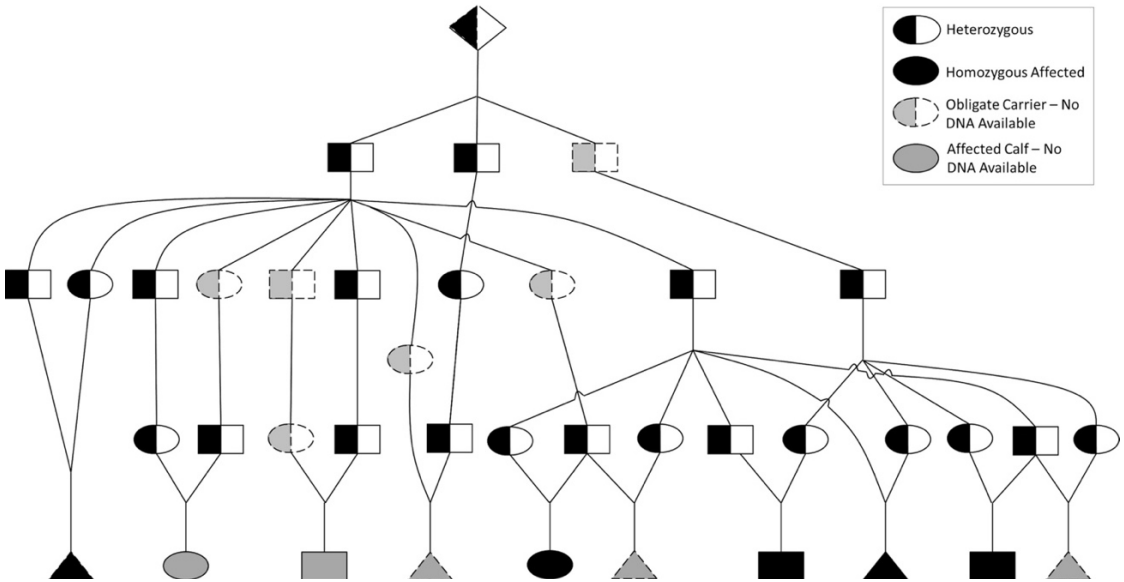

Supplement Table 2 (S2 Table). Variants in region of homozygosity in MD affected calves on chromosome 26

Chromosome	Position	Reference	Alternative	RefSNP Identifier	Additional RefSNP Identifier
chr26	10376787	T	C	rs210955452	
chr26	10377627	A	G	rs209706971	
chr26	10379807	C	T	rs378899958	
chr26	10382198	A	T	rs109097749	
chr26	10382642	C	T	rs382266037	
chr26	10382754	T	C	rs136944293	
chr26	10386634	T	C	rs133310339	
chr26	10390353	G	A	rs136544440	
chr26	10390433	C	T	rs133679469	
chr26	10390472	A	G	rs110697357	
chr26	10390595	G	A	rs132759718	
chr26	10390780	A	G	rs109715996	
chr26	10390858	G	A	rs135266051	
chr26	10390951	T	G	rs132712217	
chr26	10393249	TATC	CATA	rs133761579	rs135203078
chr26	10393267	T	C	rs133045904	
chr26	10393346	G	A	rs133615020	
chr26	10393693	G	A	rs134948945	
chr26	10393786	G	A	rs109504372	
chr26	10394854	C	T	rs135353135	
chr26	10394947	C	T	rs133279700	
chr26	10395741	T	C	rs42776147	
chr26	10396177	G	A	rs110022796	
chr26	10396197	C	T	rs134654665	
chr26	10396356	T	G	rs109103681	
chr26	10397043	A	G	rs210653396	
chr26	10397632	CA	TG	rs136064809	rs132815911
chr26	10397846	C	T	rs134682392	
chr26	10398562	C	T	rs137641807	
chr26	10398855	C	T	rs208019613	
chr26	10398943	C	T	rs135761829	
chr26	10399044	A	G	rs384541939	

chr26	10399621	T	G	rs132694323	
chr26	10401952	G	A	rs134173247	
chr26	10402170	A	G	rs133518748	
chr26	10404538	T	A	rs110381322	
chr26	10404570	C	T	rs110445481	
chr26	10405263	A	C	rs110624917	
chr26	10405356	C	T	rs134252679	
chr26	10405527	C	T	rs109149630	
chr26	10405639	C	A	rs110412863	
chr26	10405660	A	G	rs109803403	
chr26	10406016	A	G	rs111030789	
chr26	10406057	CCG	CTCG	rs136102214	
chr26	10406066	C	T	rs136764510	
chr26	10406076	T	A	rs134764304	
chr26	10412655	C	T	rs381724703	
chr26	10413143	G	A	rs134294643	
chr26	10547204	G	A	rs209288570	
chr26	10549508	G	A	rs211153422	
chr26	10550523	C	T	rs208824523	
chr26	10557362	G	C	rs386125137	
chr26	10557489	GAAAAAAAACTC	GAAAAACTC	rs380608197	
chr26	10560049	T	C	rs378952040	
chr26	10565447	C	T	rs209276038	
chr26	10577143	C	T	rs209276038	
chr26	10580678	T	C	rs210490933	
chr26	10583079	C	A	rs208019016	
chr26	10583136	T	A	rs210465256	
chr26	10583156	G	C	rs208095283	
chr26	10583356	TAATC	TATC	rs383612390	
chr26	10584897	G	A	rs209568780	
chr26	10584983	C	T	rs136430637	
chr26	10587751	A	G	rs209161634	
chr26	10588055	C	A	rs210043061	
chr26	10588068	G	A	rs207649025	
chr26	10588110	A	G	rs133140703	
chr26	10588399	TTTTT	TTTTA	rs461559046	
chr26	10588658	A	G	rs208982519	

chr26	10588677	T	C	rs210849526	
chr26	10588687	C	T	rs211035015	
chr26	10588711	C	T	rs207742593	
chr26	10588792	A	T	rs209389241	
chr26	10588802	C	G	rs209151405	
chr26	10589465	C	T	rs209814244	
chr26	10589647	C	T	rs209504774	
chr26	10589656	C	T	rs211324469	
chr26	10589716	G	T	rs208084472	
chr26	10590013	A	G	rs211458518	
chr26	10590264	G	C	rs208996657	
chr26	10590411	TCCCTG	TCCCCTG	rs443287848	
chr26	10590502	T	G	rs384953353	
chr26	10590509	T	C	rs379374948	
chr26	10590791	TT	CA	rs207829503	rs382701105
chr26	10591506	C	T	rs208898144	
chr26	10591521	A	G	rs135070334	
chr26	10593024	T	C	rs208108268	
chr26	10593367	T	A	rs209511448	
chr26	10594300	T	C	rs211633714	
chr26	10594730	T	C	rs377983575	
chr26	10595930	G	C	rs211667365	
chr26	10597618	G	A	rs208962457	
chr26	10597694	G	A	rs383414419	
chr26	10597723	T	C	rs378769066	
chr26	10597811	A	G	rs381113509	
chr26	10597925	A	G	rs384994123	
chr26	10598282	T	C	rs378593721	
chr26	10598384	CA	AG	rs384789949	rs378857720
chr26	10598446	C	T	rs797719515	
chr26	10598585	G	T	rs382397051	
chr26	10598631	G	T	rs384464525	
chr26	10598678	A	G	rs379876101	
chr26	10598770	GCT	CCA	rs382853026	rs457467257
chr26	10598974	C	T	rs382141898	
chr26	10599149	C	T	rs209389741	
chr26	10599474	G	A	rs209885360	
chr26	10600597	C	A	rs210442194	

chr26	10601002	T	C	rs380267862	
chr26	10601008	G	A	rs211009517	
chr26	10601060	TG	CA	rs386102929	rs380672529
chr26	10601117	G	A	rs211329313	
chr26	10616433	C	T	-	
chr26	10653007	A	T	rs385112219	
chr26	10685280	C	T	rs110633870	
chr26	10713132	G	A	rs383233592	
chr26	10956261	A	G	rs136478478	
chr26	10956439	C	T	rs109489086	
chr26	10959863	G	A	rs42087142	
chr26	10960055	G	A	rs42087145	
chr26	10960104	C	T	rs42087146	
chr26	10961328	TAATT	TATT	rs449279135	
chr26	10962811	C	T	rs42087154	
chr26	10964731	C	T	rs42087164	
chr26	10964813	CGGC	TGGC	rs209806893	
chr26	10964972	C	A	rs42087166	
chr26	10965393	G	A	rs208894229	
chr26	10965399	A	C	rs209670306	
chr26	10966728	GAGGAAG	GAGAAAG	rs42087175	
chr26	10967597	T	C	rs42087178	
chr26	10968136	C	T	rs42087179	
chr26	10979515	T	C	rs209401636	
chr26	10982292	TGAGAGAGGAT	TGAGAGGAT	-	
chr26	14404993	T	C	-	
chr26	15898152	C	T	-	

Table 2. Candidate variants identified with WGS data

Candidate variants identified from whole genome sequence data of 3 affected calves, 10 obligate carriers, and 7 related individuals, further filtered using WGS data from 4,997 additional animals from other laboratory projects, the American Hereford Association, and public databases. The missense variant (bold) is located in *CYP26C1* and is predicted to be deleterious to gene or protein function.

Chromosome	**Position**	**Reference**	**Alternative**	**Variant effect predictor consequence**	**rs Identifier**
7	15413	CAACT	TAACT	Intergenic variant	-
26	10588399	TTTTT	TTTTA	Intron variant	rs461559046
26	10616433	C	T	Downstream gene variant	-
26	10713132	G	A	Downstream gene variant	-
26	10794674	G	A	Intergenic variant	-
26	10982292	TGAGAGAGGAT	TGAGAGGAT	Intron variant	-
26	14404993	T	C	Missense variant (p.L188P; SIFT=0, deleterious)	-
26	15898152	C	T	Upstream gene variant	-

Table 3. Genotyping of the variant Chr26 g.14404993T>C

Given is the count of individuals by classification for each genotype. All animals with the CC genotype were affected with MD. All parents of affected MD calves had a TC genotype.

Reporting Herd 1	**TT**	**TC**	**CC**	**Total Animals**
Founder in either maternal or paternal pedigree	95	50	0	145
Founder in both maternal and paternal pedigree	2	5	2	9
No ties to founder	91	0	0	91
Total Herd 1	188	55	2	245
Reporting Herd 2				
Founder in either maternal or paternal pedigree	114	35	0	149
Founder in both maternal and paternal pedigree	4	5	1	10
No ties to founder	239	0	0	239
Total Herd 2	357	40	1	398
Other				
Founder in either maternal or paternal pedigree	13	20	0	33
Founder in both maternal and paternal pedigree	48	37	2	87
No ties to founder	18	0	0	18
Animal is founder	0	1	0	1
Total Other Genotypes	79	58	2	139
Total Animals Genotyped	**624**	**153**	**5**	**782**

Table 4. CYP26C1 Genotyping (Chr26 g.14404993T>C) by source

* Samples detailed in Table 3

***CYP26C1* Genotype Source**	**Animals Genotyped**
WGS animals for this project *	20
Hereford cattle genotyped for this project *	762
Other WGS variant data generated in our lab	101
1000 bulls (Daetwyler et al., 2014) and American Hereford Association (WGS)	1705
Sequence Read Archive	783
Total	**3,371**

Supplement Table 3 (S3 Table). Droplet Digital PCR Proportion of Variant Alleles

Sample	**Proportion of Variant Alleles**	**St Dev**
Reference Control	0.0009	0.0007
Variant Control	0.9984	0.0009
Heterozygous Control	0.4937	0.0026
Suspect Founder	0.5027	0.0127
Sire of Suspect Founder	0.0006	0.0003
Maternal Grandsire of Suspect Founder	0.0006	0.0009
Sire of Maternal Granddam of Suspect Founder	0.0014	0.0006

Figure 3. Conservation of the CYP26C1 protein across species

Shown is a portion of the CYP26C1 protein (amino acids 151 to 200 of 523 in the ARS-UCD1.2 reference assembly). Amino acid 188 (bold), altered in Mandibulofacial Dysostosis calves, is conserved across all other species studied.

	151				200
Bos taurus MD affected	RAALECYVPR	LQRALRREVR	SWCAARGPVA	VYEAAKA**P**TF	RMAARILLGL
Bos taurus reference	RAALECYVPR	LQRALRREVR	SWCAARGPVA	VYEAAKA**L**TF	RMAARILLGL
Ovis aries	RAALERYVPR	LQGALRREVR	SWCAARGPVA	VYEAAKA**L**TF	RMAARILLGL
Sus scrofa	RAALERYVPR	LQGALRREVR	SWCVARGPVA	VYEAAKA**L**TF	RMAARILLGL
Equus caballus	RAALERYVPR	LQGALRREVR	SWCAARGPVA	VYEAAKA**L**TF	RMAARILLGL
Homo sapiens	RAALERYVPR	LQGALRHEVR	SWCAAGGPVS	VYDASKA**L**TF	RMAARILLGL
Canis lupus familiaris	RAALQRLVPR	LQGALRREVR	SWCAARRPVA	VYQAAKA**L**TF	RMAARILLGL
Mus musculus	RSSLEQFVPR	LQGALRREVR	SWCAAQRPVA	VYQAAKA**L**TF	RMAARILLGL
Gallus gallus domesticus	RAALESYLPR	IQKVVSWELR	GWCMQPGSIA	VYSSAKT**L**TF	RIAARILLGL
Danio rerio	RGALEAYLTR	LQDVVKSEIA	KWCTETGSVE	VYTAAKS**L**TF	RIAVRVLLGL
Xenopus tropicalis	SAALESYLPR	IHEAVRWEVR	SWCRGVGPVS	MLSCAKA**L**TF	RIAARILLGL

Figure 4. Structural modeling of cytochrome CYP26C1

A. Three-dimensional structural model of CYP26C1 (B. taurus) showing the heme in red ball, all trans-retinoic acid (atRA) in green stick and the L188P mutation in magenta stick. B. The active site focused structure. C. The secondary structure prediction of the wild-type L188 segment (positions 179–200). D. The secondary structure prediction of the 179–200 segment with the L188P mutation. In (C, D), the red bars (jnetpred) indicate the predicted position of a helix, which is broken in the presence of the L188P mutation. Confidence in the predicted structure (JNETCONF) is displayed by vertical black bars.

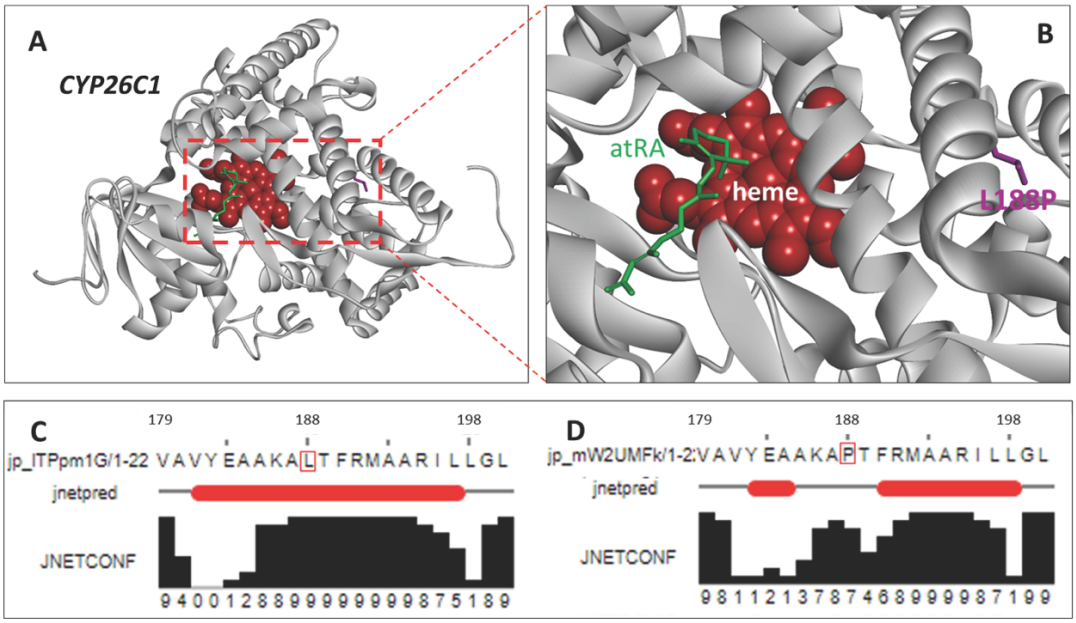

REFERENCES

Adams, H. A., T. S. Sonstegard, P. M. VanRaden, D. J. Null, C. P. Van Tassell, D. M. Larkin, and H. A. Lewin. 2016. Identification of a nonsense mutation in APAF1 that is likely causal for a decrease in reproductive efficiency in Holstein dairy cattle. Journal of Dairy Science. 99:6693–6701. doi:https://doi.org/10.3168/jds.2015-10517.

Adeola, O., R. O. Ball, and L. G. Young. 1992. Porcine Skeletal Muscle Myofibrillar Protein Synthesis is Stimulated by Ractopamine. The Journal of Nutrition. 122:488–495. doi:10.1093/jn/122.3.488.

Adhihetty, P. J., I. Irrcher, A.-M. Joseph, V. Ljubicic, and D. A. Hood. 2003. Plasticity of Skeletal Muscle Mitochondria in Response to Contractile Activity. Experimental Physiology. 88:99–107. doi:10.1113/eph8802505.

Agerholm, J. S., F. J. McEvoy, S. Heegaard, C. Charlier, V. Jagannathan, and C. Drögemüller. 2017. A de novo missense mutation of FGFR2 causes facial dysplasia syndrome in Holstein cattle. BMC Genetics. 18:1–9. doi:10.1186/s12863-017-0541-3.

Ahmed, M. K., X. Ye, and P. J. Taub. 2016. Review of the Genetic Basis of Jaw Malformations. Journal of pediatric genetics. 5:209–219. doi:10.1055/s-0036-1593505.

Anderson, P. T., W. G. Helferich, L. C. Parkhill, R. A. Merkel, and W. G. Bergen. 1990. Ractopamine Increases Total and Myofibrillar Protein Synthesis in Cultured Rat Myotubes. The Journal of Nutrition. 120:1677–1683. doi:10.1093/jn/120.12.1677.

Azad, M. A. K., M. Kikusato, S. Sudo, T. Amo, and M. Toyomizu. 2010. Time course of ROS production in skeletal muscle mitochondria from chronic heat-exposed broiler chicken. Comparative Biochemistry and Physiology Part A: Molecular & Integrative Physiology. 157:266–271. doi:10.1016/j.cbpa.2010.07.011.

Barnes, T. L., C. N. Cadaret, K. A. Beede, T. B. Schmidt, J. L. Petersen, and D. T. Yates. 2019. Hypertrophic muscle growth and metabolic efficiency were impaired by chronic heat stress, improved by zilpaterol supplementation, and not affected by ractopamine supplementation in feedlot lambs1. Journal of Animal Science. 97:4101–4113. doi:10.1093/jas/skz271.

Basarab, J. A., M. A. Price, J. L. Aalhus, E. K. Okine, W. M. Snelling, and K. L. Lyle. 2003. Residual feed intake and body composition in young growing cattle. Can. J. Anim. Sci. 83:189–204. doi:10.4141/A02-065.

Bassols, A., C. Costa, P. D. Eckersall, J. Osada, J. Sabrià, and J. Tibau. 2014. The pig as an animal model for human pathologies: A proteomics perspective. PROTEOMICS – Clinical Applications. 8:715–731. doi:10.1002/prca.201300099.

Baumgard, L. H., and R. P. Rhoads. 2013. Effects of Heat Stress on Postabsorptive Metabolism and Energetics. Annu. Rev. Anim. Biosci. 1:311–337. doi:10.1146/annurev-animal-031412-103644.

Beede, D. K., and R. J. Collier. 1986. Potential Nutritional Strategies for Intensively Managed Cattle during Thermal Stress. Journal of Animal Science. 62:543–554. doi:10.2527/jas1986.622543x.

Bergen, W. G., S. E. Johnson, D. M. Skjaerlund, A. S. Babiker, N. K. Ames, R. A. Merkel, and D. B. Anderson. 1989. Muscle Protein Metabolism in Finishing Pigs Fed Ractopamine. Journal of Animal Science. 67:2255–2262. doi:10.2527/jas1989.6792255x.

Bernabucci, U., N. Lacetera, L. H. Baumgard, R. P. Rhoads, B. Ronchi, and A. Nardone. 2010. Metabolic and hormonal acclimation to heat stress in domesticated ruminants. Animal. 4:1167–1183. doi:10.1017/S175173111000090X.

Bottje, W. G., and G. E. Carstens. 2009. Association of mitochondrial function and feed efficiency in poultry and livestock species1. Journal of Animal Science. 87:E48–E63. doi:10.2527/jas.2008-1379.

Boyd, B. M., S. D. Shackelford, K. E. Hales, T. M. Brown-Brandl, M. L. Bremer, M. L. Spangler, T. L. Wheeler, D. A. King, and G. E. Erickson. 2015. Effects of shade and feeding zilpaterol hydrochloride to finishing steers on performance, carcass quality, heat stress, mobility, and body temperature1. Journal of Animal Science. 93:5801–5811. doi:10.2527/jas.2015-9613.

Braun, M., A. Lehmbecker, D. Eikelberg, M. Hellige, A. Beineke, J. Metzger, and O. Distl. 2021. De novo ZIC2 frameshift variant associated with frontonasal dysplasia in a Limousin calf. BMC Genomics. 22:1. doi:10.1186/s12864-020-07350-y.

Brown, D., K. Ryan, Z. Daniel, M. Mareko, R. Talbot, J. Moreton, T. C. B. Giles, R. Emes, C. Hodgman, T. Parr, and J. M. Brameld. 2018. The Beta-adrenergic agonist, Ractopamine, increases skeletal muscle expression of Asparagine Synthetase as part of an integrated stress response gene program. Scientific Reports. 8:15915. doi:10.1038/s41598-018-34315-9.

Brownstein, A. J., S. Ganesan, C. M. Summers, S. Pearce, B. J. Hale, J. W. Ross, N. Gabler, J. T. Seibert, R. P. Rhoads, L. H. Baumgard, and J. T. Selsby. 2017. Heat stress causes dysfunctional autophagy in oxidative skeletal muscle. Physiological Reports. 5:e13317. doi:10.14814/phy2.13317.

Bryan, B. A., D. Li, X. Wu, and M. Liu. 2005. The Rho family of small GTPases: crucial regulators of skeletal myogenesis. CMLS, Cell. Mol. Life Sci. 62:1547–1555. doi:10.1007/s00018-005-5029-z.

Buntyn, J. O., N. C. Burdick Sanchez, T. B. Schmidt, G. E. Erickson, S. E. Sieren, S. J. Jones, and J. A. Carroll. 2016. The metabolic, stress axis, and hematology response of

zilpaterol hydrochloride supplemented beef heifers when exposed to a dual corticotropin-releasing hormone and vasopressin challenge1,2,3. Journal of Animal Science. 94:2798–2810. doi:10.2527/jas.2015-0192.

Burrack, R. M., E. M. Duffy, D. T. Yates, T. B. Schmidt, and J. L. Petersen. 2020. Whole blood transcriptome analysis in feedlot cattle after 35 days of supplementation with a β1-adrenergic agonist. J Appl Genetics. 61:117–121. doi:10.1007/s13353-019-00527-6.

Cadaret, C. N., K. A. Beede, H. E. Riley, and D. T. Yates. 2017. Acute exposure of primary rat soleus muscle to zilpaterol HCl (β2 adrenergic agonist), TNFα, or IL-6 in culture increases glucose oxidation rates independent of the impact on insulin signaling or glucose uptake. Cytokine. 96:107–113. doi:10.1016/j.cyto.2017.03.014.

Cairns, S. P., and F. Borrani. 2015. β-Adrenergic modulation of skeletal muscle contraction: key role of excitation-contraction coupling. J Physiol. 593:4713–4727. doi:10.1113/JP270909.

Celi, P. 2011. Oxidative Stress in Ruminants. In: L. Mandelker and P. Vajdovich, editors. Studies on Veterinary Medicine. Humana Press, Totowa, NJ. p. 191–231. Available from: 10.1007/978-1-61779-071-3_13

Cepero, M., J. C. Cubría, R. Reguera, R. Balaña-Fouce, C. Ordónez, and D. Ordóñez. 1998. Plasma and Muscle Polyamine Levels in Aerobically Exercised Rats Treated with Salbutamol. Journal of Pharmacy and Pharmacology. 50:1059–1064. doi:10.1111/j.2042-7158.1998.tb06922.x.

Chauhan, S. S., P. Celi, B. J. Leury, I. J. Clarke, and F. R. Dunshea. 2014. Dietary antioxidants at supranutritional doses improve oxidative status and reduce the negative effects of heat stress in sheep1,2. Journal of Animal Science. 92:3364–3374. doi:10.2527/jas.2014-7714.

Chen, Q., Y. Zhao, G. Shen, and J. Dai. 2018. Etiology and Pathogenesis of Hemifacial Microsomia. Journal of Dental Research. 97:1297–1305. doi:10.1177/0022034518795609.

Ciepłoch, A., K. Rutkowska, J. Oprządek, and E. Poławska. 2017. Genetic disorders in beef cattle: a review. Genes Genom. 39:461–471. doi:10.1007/s13258-017-0525-8.

Cingolani, P., A. Platts, L. L. Wang, M. Coon, T. Nguyen, L. Wang, S. J. Land, X. Lu, and D. M. Ruden. 2012. A program for annotating and predicting the effects of single nucleotide polymorphisms, SnpEff: SNPs in the genome of Drosophila melanogaster strain w1118; iso-2; iso-3. Fly. 6:80–92. doi:10.4161/fly.19695.

Daetwyler, H. D., A. Capitan, H. Pausch, P. Stothard, R. Van Binsbergen, R. F. Brøndum, X. Liao, A. Djari, S. C. Rodriguez, C. Grohs, D. Esquerré, O. Bouchez, M. N. Rossignol, C. Klopp, D. Rocha, S. Fritz, A. Eggen, P. J. Bowman, D. Coote, A. J. Chamberlain, C. Anderson, C. P. Vantassell, I. Hulsegge, M. E. Goddard, B.

Guldbrandtsen, M. S. Lund, R. F. Veerkamp, D. A. Boichard, R. Fries, and B. J. Hayes. 2014. Whole-genome sequencing of 234 bulls facilitates mapping of monogenic and complex traits in cattle. Nature Genetics. 46:858–865. doi:10.1038/ng.3034.

Dawes Matthew, Chowienczyk Philip J., and Ritter James M. 1997. Effects of Inhibition of the l-Arginine/Nitric Oxide Pathway on Vasodilation Caused by β-Adrenergic Agonists in Human Forearm. Circulation. 95:2293–2297. doi:10.1161/01.CIR.95.9.2293.

Depew, M. J., C. A. Simpson, M. Morasso, and J. L. R. Rubenstein. 2005. Reassessing the Dlx code: the genetic regulation of branchial arch skeletal pattern and development. Journal of Anatomy. 207:501–561. doi:10.1111/j.1469-7580.2005.00487.x.

Derno, M., G. Nürnberg, and B. Kuhla. 2019. Characterizing the metabotype and its persistency in lactating Holstein cows: An approach toward metabolic efficiency measures. Journal of Dairy Science. 102:6559–6570. doi:10.3168/jds.2019-16274.

Divakaruni, A. S., A. Paradyse, D. A. Ferrick, A. N. Murphy, and M. Jastroch. 2014. Analysis and Interpretation of Microplate-Based Oxygen Consumption and pH Data. In: Methods in Enzymology. Vol. 547. Elsevier. p. 309–354. Available from: https://linkinghub.elsevier.com/retrieve/pii/B9780128014158000163

Dobin, A., C. A. Davis, F. Schlesinger, J. Drenkow, C. Zaleski, S. Jha, P. Batut, M. Chaisson, and T. R. Gingeras. 2013. STAR: ultrafast universal RNA-seq aligner. Bioinformatics. 29:15–21. doi:10.1093/bioinformatics/bts635.

Drögemüller, C., H. Kuiper, M. Peters, S. Guionaud, O. Distl, and T. Leeb. 2002. Congenital hypotrichosis with anodontia in cattle: A genetic, clinical and histological analysis. Veterinary Dermatology. 13:307–313. doi:10.1046/j.1365-3164.2002.00313.x.

Elam, N. A., J. T. Vasconcelos, G. Hilton, D. L. VanOverbeke, T. E. Lawrence, T. H. Montgomery, W. T. Nichols, M. N. Streeter, J. P. Hutcheson, D. A. Yates, and M. L. Galyean. 2009. Effect of zilpaterol hydrochloride duration of feeding on performance and carcass characteristics of feedlot cattle. J Anim Sci. 87:2133–2141. doi:10.2527/jas.2008-1563.

Ely, B. R., A. T. Lovering, M. Horowitz, and C. T. Minson. 2014. Heat acclimation and cross tolerance to hypoxia: Bridging the gap between cellular and systemic responses. Temperature. 1:107–114. doi:10.4161/temp.29800.

Ganesan, S., C. Reynolds, K. Hollinger, S. C. Pearce, N. K. Gabler, L. H. Baumgard, R. P. Rhoads, and J. T. Selsby. 2016. Twelve hours of heat stress induces inflammatory signaling in porcine skeletal muscle. American Journal of Physiology-Regulatory, Integrative and Comparative Physiology. 310:R1288–R1296. doi:10.1152/ajpregu.00494.2015.

Ganesan, S., C. M. Summers, S. C. Pearce, N. K. Gabler, R. J. Valentine, L. H. Baumgard, R. P. Rhoads, and J. T. Selsby. 2017. Short-term heat stress causes altered

intracellular signaling in oxidative skeletal muscle1. Journal of Animal Science. 95:2438–2451. doi:10.2527/jas.2016.1233.

Ganesan, S., C. M. Summers, S. C. Pearce, N. K. Gabler, R. J. Valentine, L. H. Baumgard, R. P. Rhoads, and J. T. Selsby. 2018. Short-term heat stress altered metabolism and insulin signaling in skeletal muscle. Journal of Animal Science. 96:154–167. doi:10.1093/jas/skx083.

Gentile, A., and S. Testoni. 2006. Inherited disorders of cattle: a selected review. Slov vet res. 43:17–29.

Geraert, P. A., J. C. F. Padilha, and S. Guillaumin. 1996. Metabolic and endocrine changes induced by chronic heatexposure in broiler chickens: growth performance, body composition and energy retention. British Journal of Nutrition. 75:195–204. doi:10.1017/BJN19960124.

Gitton, Y., É. Heude, M. Vieux-Rochas, L. Benouaiche, A. Fontaine, T. Sato, Y. Kurihara, H. Kurihara, G. Couly, and G. Levi. 2010. Evolving maps in craniofacial development. Seminars in Cell and Developmental Biology. 21:301–308. doi:10.1016/j.semcdb.2010.01.008.

Gonzalez, J. M., J. N. Carter, D. D. Johnson, S. E. Ouellette, and S. E. Johnson. 2007. Effect of ractopamine-hydrochloride and trenbolone acetate on longissimus muscle fiber area, diameter, and satellite cell numbers in cull beef cows1. Journal of Animal Science. 85:1893–1901. doi:10.2527/jas.2006-624.

Gonzalez, J. M., R. D. Dijkhuis, D. D. Johnson, J. N. Carter, and S. E. Johnson. 2008. Differential response of cull cow muscles to the hypertrophic actions of ractopamine-hydrogen chloride1. Journal of Animal Science. 86:3568–3574. doi:10.2527/jas.2008-1049.

Gonzalez, J. M., S. E. Johnson, A. M. Stelzleni, T. A. Thrift, J. D. Savell, T. M. Warnock, and D. D. Johnson. 2010. Effect of ractopamine–HCl supplementation for 28 days on carcass characteristics, muscle fiber morphometrics, and whole muscle yields of six distinct muscles of the loin and round. Meat Science. 85:379–384. doi:10.1016/j.meatsci.2010.02.004.

Gonzalez-Rivas, P. A., S. S. Chauhan, M. Ha, N. Fegan, F. R. Dunshea, and R. D. Warner. 2020. Effects of heat stress on animal physiology, metabolism, and meat quality: A review. Meat Science. 162:108025. doi:10.1016/j.meatsci.2019.108025.

Granstrom, G., G. Zellin, B. C. Magnusson, and H. Mangs. 1988. Enzyme histochemical analysis of Meckel's cartilage. Journal of Anatomy. 160:101–108.

Grubbs, J. K., A. N. Fritchen, E. Huff-Lonergan, J. C. M. Dekkers, N. K. Gabler, and S. M. Lonergan. 2013. Divergent genetic selection for residual feed intake impacts

mitochondria reactive oxygen species production in pigs1. Journal of Animal Science. 91:2133–2140. doi:10.2527/jas.2012-5894.

Gruber, S. L., J. D. Tatum, T. E. Engle, M. A. Mitchell, S. B. Laudert, A. L. Schroeder, and W. J. Platter. 2007. Effects of ractopamine supplementation on growth performance and carcass characteristics of feedlot steers differing in biological type. Journal of Animal Science. 85:1809–1815. doi:10.2527/jas.2006-634.

Guengerich, F. P. 2015. Human Cytochrome P450 Enzymes. In: P. R. Ortiz de Montellano, editor. Cytochrome P450: Structure, Mechanism, and Biochemistry. Springer International Publishing, Cham. p. 523–785. Available from: https://doi.org/10.1007/978-3-319-12108-6_9

Gunawan, A. M., B. T. Richert, A. P. Schinckel, A. L. Grant, and D. E. Gerrard. 2007. Ractopamine induces differential gene expression in porcine skeletal muscles1. Journal of Animal Science. 85:2115–2124. doi:10.2527/jas.2006-540.

Hao, Yue, Y. Feng, P. Yang, Y. Cui, J. Liu, C. Yang, and X. Gu. 2016. Transcriptome analysis reveals that constant heat stress modifies the metabolism and structure of the porcine longissimus dorsi skeletal muscle. Mol Genet Genomics. 291:2101–2115. doi:10.1007/s00438-016-1242-8.

Hao, Y., J. R. Liu, Y. Zhang, P. G. Yang, Y. J. Feng, Y. J. Cui, C. H. Yang, and X. H. Gu. 2016. The microRNA expression profile in porcine skeletal muscle is changed by constant heat stress. Animal Genetics. 47:365–369. doi:10.1111/age.12419.

Hergenreder, J. E., J. F. Legako, T. T. N. Dinh, P. R. Broadway, K. S. Spivey, J. O. Baggerman, J. P. Hutcheson, M. E. Corrigan, and B. J. Johnson. 2017. Zilpaterol Hydrochloride affects Cellular Muscle Metabolism and Lipid Components of 10 Different Muscles in Feedlot Heifers. Meat and Muscle Biology. 1. doi:10.22175/mmb2017.02.0013. Available from: https://www.iastatedigitalpress.com/mmb/article/pubid/2017-02-0013/

Johnston, A. D., C. A. Simões-Pires, T. V. Thompson, M. Suzuki, and J. M. Greally. 2019. Functional genetic variants can mediate their regulatory effects through alteration of transcription factor binding. Nature Communications. 10:3472. doi:10.1038/s41467-019-11412-5.

Kedishvili, N. Y. 2013. Enzymology of retinoic acid biosynthesis and degradation. Journal of Lipid Research. 54:1744–1760. doi:10.1194/jlr.R037028.

Kellermeier, J. D., A. W. Tittor, J. C. Brooks, M. L. Galyean, D. A. Yates, J. P. Hutcheson, W. T. Nichols, M. N. Streeter, B. J. Johnson, and M. F. Miller. 2009. Effects of zilpaterol hydrochloride with or without an estrogen-trenbolone acetate terminal implant on carcass traits, retail cutout, tenderness, and muscle fiber diameter in finishing steers1. Journal of Animal Science. 87:3702–3711. doi:10.2527/jas.2009-1823.

Kim, M. K., and Y. K. Kang. 1999. Positional preference of proline in α-helices. Protein Science. 8:1492–1499. doi:10.1110/ps.8.7.1492.

Kolath, W. H., M. S. Kerley, J. W. Golden, and D. H. Keisler. 2006. The relationship between mitochondrial function and residual feed intake in Angus steers1. Journal of Animal Science. 84:861–865. doi:10.2527/2006.844861x.

Kolde, R. 2012. Pheatmap: pretty heatmaps. R package version. 1. Available from: https://www.rdocumentation.org/packages/pheatmap

Kubik, R. M., S. M. Tietze, T. B. Schmidt, D. T. Yates, and J. L. Petersen. 2018. Investigation of the skeletal muscle transcriptome in lambs fed β adrenergic agonists and subjected to heat stress for 21 d1. Translational Animal Science. 2:S53–S56. doi:10.1093/tas/txy053.

Kühnel, K., N. Ke, M. J. Cryle, S. G. Sligar, M. A. Schuler, and I. Schlichting. 2008. Crystal Structures of Substrate-Free and Retinoic Acid-Bound Cyanobacterial Cytochrome P450 CYP120A1. Biochemistry. 47:6552–6559. doi:10.1021/bi800328s.

Kumar, C. R., H. A. Shaikh, A. V Kandarpalle, and K. Allure. Surgical Correction of Congenital Macrostomia in Cattle Calf.

Lammer, E. J., D. T. Chen, R. M. Hoar, N. D. Agnish, P. J. Benke, J. T. Braun, C. J. Curry, P. M. Fernhoff, A. W. Grix Jr, and I. T. Lott. 1985. Retinoic acid embryopathy. New England Journal of Medicine. 313:837–841.

Lean, I. J., J. M. Thompson, and F. R. Dunshea. 2014. A Meta-Analysis of Zilpaterol and Ractopamine Effects on Feedlot Performance, Carcass Traits and Shear Strength of Meat in Cattle. B. Kaltenboeck, editor. PLoS ONE. 9:e115904. doi:10.1371/journal.pone.0115904.

Lee, B. H., F. Morice-Picard, F. Boralevi, B. Chen, and R. J. Desnick. 2018. Focal facial dermal dysplasia type 4: Identification of novel CYP26C1 mutations in unrelated patients. Journal of Human Genetics. 63:257–261. doi:10.1038/s10038-017-0375-x.

Lee, B.-K., A. A. Bhinge, A. Battenhouse, R. M. McDaniell, Z. Liu, L. Song, Y. Ni, E. Birney, J. D. Lieb, T. S. Furey, G. E. Crawford, and V. R. Iyer. 2012. Cell-type specific and combinatorial usage of diverse transcription factors revealed by genome-wide binding studies in multiple human cells. Genome Res. 22:9–24. doi:10.1101/gr.127597.111.

Lee, N. K. L., and H. E. MacLean. 2011. Polyamines, androgens, and skeletal muscle hypertrophy. J Cell Physiol. 226:1453–1460. doi:10.1002/jcp.22569.

Lefkowitz, R. J., J. M. Stadel, and M. G. Caron. 1983. Adenylate Cyclase-Coupled Beta-Adrenergic Receptors: Structure and Mechanisms of Activation and Desensitization. Annu. Rev. Biochem. 52:159–186. doi:10.1146/annurev.bi.52.070183.001111.

Li, H. 2013. Aligning sequence reads, clone sequences and assembly contigs with BWA-MEM. 00:1–3.

Li, H., C. Gariépy, Y. Jin, M. Font i Furnols, J. Fortin, L. M. Rocha, and L. Faucitano. 2015. Effects of ractopamine administration and castration method on muscle fiber characteristics and sensory quality of the longissimus muscle in two Piétrain pig genotypes. Meat Science. 102:27–34. doi:10.1016/j.meatsci.2014.10.027.

Li, H., B. Handsaker, A. Wysoker, T. Fennell, J. Ruan, N. Homer, G. Marth, G. Abecasis, R. Durbin, and 1000 Genome Project Data Processing Subgroup. 2009. The Sequence Alignment/Map format and SAMtools. Bioinformatics. 25:2078–2079. doi:10.1093/bioinformatics/btp352.

Li, R., Z. Jia, and M. A. Trush. 2016. Defining ROS in Biology and Medicine. React Oxyg Species (Apex). 1:9–21. doi:10.20455/ros.2016.803.

Lines, M. A., L. Huang, J. Schwartzentruber, S. L. Douglas, D. C. Lynch, C. Beaulieu, M. L. Guion-Almeida, R. M. Zechi-Ceide, B. Gener, and G. Gillessen-Kaesbach. 2012. Haploinsufficiency of a spliceosomal GTPase encoded by EFTUD2 causes mandibulofacial dysostosis with microcephaly. The American Journal of Human Genetics. 90:369–377. doi:10.1016/j.ajhg.2011.12.023.

Lohse, M. J., J. L. Benovic, M. G. Caron, and R. J. Lefkowitz. 1990. Multiple pathways of rapid beta 2-adrenergic receptor desensitization. Delineation with specific inhibitors. J Biol Chem. 265:3202–3211.

Lopez-Carlos, M. A., R. G. Ramirez, J. I. Aguilera-Soto, A. Plascencia, H. Rodriguez, C. F. Arechiga, R. M. Rincon, C. A. Medina-Flores, and H. Gutierrez-Bañuelos. 2011. Effect of two beta adrenergic agonists and feeding duration on feedlot performance and carcass characteristics of finishing lambs. Livestock Science. 138:251–258. doi:10.1016/j.livsci.2010.12.020.

Love, M. I., W. Huber, and S. Anders. 2014. Moderated estimation of fold change and dispersion for RNA-seq data with DESeq2. Genome Biology. 15:550. doi:10.1186/s13059-014-0550-8.

Ludolph, D. C., and S. F. Konieczny. 1995. Transcription factor families: muscling in on the myogenic program. The FASEB Journal. 9:1595–1595. doi:10.1096/fasebj.9.15.8529839.

Lundby, C., J. A. L. Calbet, and P. Robach. 2009. The response of human skeletal muscle tissue to hypoxia. Cell. Mol. Life Sci. 66:3615–3623. doi:10.1007/s00018-009-0146-8.

Marcillac-Embertson, N. M., P. H. Robinson, J. G. Fadel, and F. M. Mitloehner. 2009. Effects of shade and sprinklers on performance, behavior, physiology, and the environment of heifers. Journal of Dairy Science. 92:506–517. doi:10.3168/jds.2008-1012.

Marti, S., M. Jelinski, E. Janzen, M. J. Jelinski, C. Dorin, K. Orsel, E. Pajor, J. Shearer, S. T. Millman, and K. Schwartzkopf-Genswein. 2021. A prospective longitudinal study of risk factors associated with cattle lameness in southern Alberta feedlots. Can. J. Anim. Sci. CJAS-2020-0128. doi:10.1139/CJAS-2020-0128.

Martin, M. 2011. Cutadept removes adapter sequences from high-throughput sequencing reads. EMBnet.journal. 17:10–12.

McGeady, T. A., P. J. Quinn, E. S. FitzPatrick, M. T. Ryan, D. Kilroy, and P. Lonergan. 2017. Veterinary embryology. John Wiley & Sons.

McNeel, R. L., and H. J. Mersmann. 1999. Distribution and quantification of Beta1-, Beta2-, and Beta3-adrenergic receptor subtype transcripts in porcine tissues. Journal of Animal Science. 77:611–621. doi:10.2527/1999.773611x.

Mersmann, H. J. 1998. Overview of the effects of beta-adrenergic receptor agonists on animal growth including mechanisms of action. J Anim Sci. 76:160–172. doi:10.2527/1998.761160x.

Mills, S. E. 2002. Biological basis of the ractopamine response. Journal of Animal Science. 80:E28–E32. doi:10.2527/animalsci2002.80E-Suppl_2E28x.

Mitlöhner, F. M., M. L. Galyean, and J. J. McGlone. 2002. Shade effects on performance, carcass traits, physiology, and behavior of heat-stressed feedlot heifers1. Journal of Animal Science. 80:2043–2050. doi:10.1093/ansci/80.8.2043.

Mitlöhner, F. M., J. L. Morrow, J. W. Dailey, S. C. Wilson, M. L. Galyean, M. F. Miller, and J. J. McGlone. 2001. Shade and water misting effects on behavior, physiology, performance, and carcass traits of heat-stressed feedlot cattle1. Journal of Animal Science. 79:2327–2335. doi:10.2527/2001.7992327x.

Møller, L. L. V., A. Klip, and L. Sylow. 2019. Rho GTPases—Emerging Regulators of Glucose Homeostasis and Metabolic Health. Cells. 8:434. doi:10.3390/cells8050434.

Montalbano, A., L. Juergensen, R. Roeth, B. Weiss, M. Fukami, S. Fricke-Otto, G. Binder, T. Ogata, E. Decker, G. Nuernberg, D. Hassel, and G. A. Rappold. 2016. Retinoic acid catabolizing enzyme CYP 26C1 is a genetic modifier in SHOX deficiency. EMBO Molecular Medicine. 8:1455–1469. doi:10.15252/emmm.201606623.

Montgomery, J. L., C. R. Krehbiel, J. J. Cranston, D. A. Yates, J. P. Hutcheson, W. T. Nichols, M. N. Streeter, D. T. Bechtol, E. Johnson, T. TerHune, and T. H. Montgomery. 2009. Dietary zilpaterol hydrochloride. I. Feedlot performance and carcass traits of steers and heifers. Journal of Animal Science. 87:1374–1383. doi:10.2527/jas.2008-1162.

Montilla, S. I. R., T. P. Johnson, S. C. Pearce, D. Gardan-Salmon, N. K. Gabler, J. W. Ross, R. P. Rhoads, L. H. Baumgard, S. M. Lonergan, and J. T. Selsby. 2014. Heat stress

causes oxidative stress but not inflammatory signaling in porcine skeletal muscle. Temperature. 1:42–50. doi:10.4161/temp.28844.

Mujahid, A., N. R. Pumford, W. Bottje, K. Nakagawa, T. Miyazawa, Y. Akiba, and M. Toyomizu. 2007. Mitochondrial Oxidative Damage in Chicken Skeletal Muscle Induced by Acute Heat Stress. The Journal of Poultry Science. 44:439–445. doi:10.2141/jpsa.44.439.

Mujahid, A., Y. Yoshiki, Y. Akiba, and M. Toyomizu. 2005. Superoxide radical production in chicken skeletal muscle induced by acute heat stress. Poultry Science. 84:307–314. doi:10.1093/ps/84.2.307.

Nakagawa, T., and L. Guarente. 2011. Sirtuins at a glance. J Cell Sci. 124:833–838. doi:10.1242/jcs.081067.

Noden, P. A. N. N. 1966. Cardiogenesis in the bovine to 35 somites.

Oryan, A., S. Shirian, and M. R. Samadian. 2011. Congenital craniofacial and skeletal defects with arthrogryposis in two newborn male Holstein Friesian calves. Comparative Clinical Pathology. 20:43–46. doi:10.1007/s00580-009-0947-z.

Papandreou, I., R. A. Cairns, L. Fontana, A. L. Lim, and N. C. Denko. 2006. HIF-1 mediates adaptation to hypoxia by actively downregulating mitochondrial oxygen consumption. Cell Metab. 3:187–197. doi:10.1016/j.cmet.2006.01.012.

Parada, C., and Y. Chai. 2015. Mandible and tongue development. In: Current topics in developmental biology. Vol. 115. Elsevier. p. 31–58.

Petersen, J. L., T. S. Kalbfleisch, M. Parris, S. M. Tietze, and J. Cruickshank. 2020. MC1R and KIT Haplotypes Associate With Pigmentation Phenotypes of North American Yak (Bos grunniens). The Journal of heredity. 111:182–193. doi:10.1093/jhered/esz070.

Petersen, J. L., S. M. Tietze, R. M. Burrack, and D. J. Steffen. 2019. Evidence for a de novo, dominant germ-line mutation causative of osteogenesis imperfecta in two Red Angus calves. Mammalian Genome. 30:81–87. doi:10.1007/s00335-019-09794-4.

Pietrosemoli, N., S. Mella, S. Yennek, M. B. Baghdadi, H. Sakai, R. Sambasivan, F. Pala, D. Di Girolamo, and S. Tajbakhsh. 2017. Comparison of multiple transcriptomes exposes unified and divergent features of quiescent and activated skeletal muscle stem cells. Skeletal Muscle. 7:28. doi:10.1186/s13395-017-0144-8.

Quinn, M. J., C. D. Reinhardt, E. R. Loe, B. E. Depenbusch, M. E. Corrigan, M. L. May, and J. S. Drouillard. 2008. The effects of ractopamine-hydrogen chloride (Optaflexx) on performance, carcass characteristics, and meat quality of finishing feedlot heifers1. Journal of Animal Science. 86:902–908. doi:10.2527/jas.2007-0117.

Ramos, P. M., C. Li, M. A. Elzo, S. E. Wohlgemuth, and T. L. Scheffler. 2020. Mitochondrial oxygen consumption in early postmortem permeabilized skeletal muscle fibers is influenced by cattle breed. Journal of Animal Science. 98:skaa044. doi:10.1093/jas/skaa044.

Rathmann, R. J., B. C. Bernhard, R. S. Swingle, T. E. Lawrence, W. T. Nichols, D. A. Yates, J. P. Hutcheson, M. N. Streeter, J. C. Brooks, M. F. Miller, and B. J. Johnson. 2012. Effects of zilpaterol hydrochloride and days on the finishing diet on feedlot performance, carcass characteristics, and tenderness in beef heifers1. Journal of Animal Science. 90:3301–3311. doi:10.2527/jas.2011-4375.

Ross, J. W., B. J. Hale, N. K. Gabler, R. P. Rhoads, A. F. Keating, and L. H. Baumgard. 2015. Physiological consequences of heat stress in pigs. Anim. Prod. Sci. 55:1381–1390. doi:10.1071/AN15267.

Ruest, L. B., X. Xiang, K. C. Lim, G. Levi, and D. E. Clouthier. 2004. Endothelin-A receptor-dependent and -independent signaling pathways in establishing mandibular identity. Development. 131:4413–4423. doi:10.1242/dev.01291.

Salin, K., S. K. Auer, B. Rey, C. Selman, and N. B. Metcalfe. 2015. Variation in the link between oxygen consumption and ATP production, and its relevance for animal performance. Proc. R. Soc. B. 282:20151028. doi:10.1098/rspb.2015.1028.

Sanz Fernandez, M. V., J. S. Johnson, M. Abuajamieh, S. K. Stoakes, J. T. Seibert, L. Cox, S. Kahl, T. H. Elsasser, J. W. Ross, S. Clay Isom, R. P. Rhoads, and L. H. Baumgard. 2015. Effects of heat stress on carbohydrate and lipid metabolism in growing pigs. Physiol Rep. 3. doi:10.14814/phy2.12315. Available from: https://www.ncbi.nlm.nih.gov/pmc/articles/PMC4393217/

Sartelet, A., T. Stauber, W. Coppieters, C. F. Ludwig, C. Fasquelle, T. Druet, Z. Zhang, N. Ahariz, N. Cambisano, T. J. Jentsch, and C. Charlier. 2014. A missense mutation accelerating the gating of the lysosomal Cl -/H+-exchanger ClC-7/Ostm1 causes osteopetrosis with gingival hamartomas in cattle. DMM Disease Models and Mechanisms. 7:119–128. doi:10.1242/dmm.012500.

Schilling, T. F., J. Sosnik, and Q. Nie. 2016. Visualizing retinoic acid morphogen gradients. Methods in Cell Biology. 133:139–163. doi:10.1016/bs.mcb.2016.03.003.

Scramlin, S. M., W. J. Platter, R. A. Gomez, W. T. Choat, F. K. McKeith, and J. Killefer. 2010. Comparative effects of ractopamine hydrochloride and zilpaterol hydrochloride on growth performance, carcass traits, and longissimus tenderness of finishing steers1. Journal of Animal Science. 88:1823–1829. doi:10.2527/jas.2009-2405.

Seahorse XF Cell Mito Stress Test Kit User Guide. 2019. Agilent User Manuals. Available from: https://www.agilent.com/cs/library/usermanuals/public/XF_Cell_Mito_Stress_Test_Kit_User_Guide.pdf

Seahorse XF Stress Test Report Generator User Guide. 2016. Agilent User Manuals. Available from: https://www.agilent.com/cs/library/usermanuals/public/XF_Stress_Test_Report_Generator_User_Guide.pdf

Serbedzija, G. N., M. Bronner-Fraser, and S. E. Fraser. 1992. Vital dye analysis of cranial neural crest cell migration in the mouse embryo. Development. 116:297–307.

Sieck, R. L., L. K. Treffer, M. Ponte Viana, O. Khalimonchuk, T. B. Schmidt, D. T. Yates, and J. L. Petersen. 2020. Beta-adrenergic agonists increase maximal output of oxidative phosphorylation in bovine satellite cells1. Translational Animal Science. 4:S94–S97. doi:10.1093/tas/txaa112.

Sillence, M. N., and M. L. Matthews. 1994. Classical and atypical binding sites for β-adrenoceptor ligands and activation of adenylyl cyclase in bovine skeletal muscle and adipose tissue membranes. British Journal of Pharmacology. 111:866–872. doi:https://doi.org/10.1111/j.1476-5381.1994.tb14818.x.

Sissom, E. K., C. D. Reinhardt, J. P. Hutcheson, W. T. Nichols, D. A. Yates, R. S. Swingle, and B. J. Johnson. 2007. Response to ractopamine-HCl in heifers is altered by implant strategy across days on feed1. Journal of Animal Science. 85:2125–2132. doi:10.2527/jas.2006-660.

Slavotinek, A. M., P. Mehrotra, I. Nazarenko, P. L. F. Tang, R. Lao, D. Cameron, B. Li, C. Chu, C. Chou, A. L. Marqueling, M. Yahyavi, K. Cordoro, I. Frieden, T. Glaser, T. Prescott, M. A. Morren, K. Devriendt, P. Y. Kwok, M. Petkovich, and R. J. Desnick. 2013. Focal facial dermal dysplasia, type IV, is caused by mutations in CYP26C1. Human Molecular Genetics. 22:696–703. doi:10.1093/hmg/dds477.

Smeitink, J., L. van den Heuvel, and S. DiMauro. 2001. The genetics and pathology of oxidative phosphorylation. Nat Rev Genet. 2:342–352. doi:10.1038/35072063.

St-Pierre, N. R., B. Cobanov, and G. Schnitkey. 2003. Economic Losses from Heat Stress by US Livestock Industries1. Journal of Dairy Science. 86:E52–E77. doi:10.3168/jds.S0022-0302(03)74040-5.

Swanson, R. M., R. G. Tait, B. M. Galles, E. M. Duffy, T. B. Schmidt, J. L. Petersen, and D. T. Yates. 2020. Heat stress-induced deficits in growth, metabolic efficiency, and cardiovascular function coincided with chronic systemic inflammation and hypercatecholaminemia in ractopamine-supplemented feedlot lambs. Journal of Animal Science. 98. doi:10.1093/jas/skaa168.

Tahayato, A., P. Dollé, and M. Petkovich. 2003. Cyp26C1 encodes a novel retinoic acid-metabolizing enzyme expressed in the hindbrain, inner ear, first branchial arch and tooth buds during murine development. Gene Expression Patterns. 3:449–454. doi:10.1016/S1567-133X(03)00066-8.

Thomsen, P. T.-N. P. D. 2003. Morphological assessmentof preimplantation embryo quality in cattle. Reproduction. 61:103–116.

Thomson, D. U., G. H. Loneragan, J. N. Henningson, S. Ensley, and B. Bawa. 2015. Description of a novel fatigue syndrome of finished feedlot cattle following transportation. Journal of the American Veterinary Medical Association. 247:66–72. doi:10.2460/javma.247.1.66.

Toyomizu, M., M. Kikusato, Y. Kawabata, M. A. K. Azad, E. Inui, and T. Amo. 2011. Meat-type chickens have a higher efficiency of mitochondrial oxidative phosphorylation than laying-type chickens. Comp Biochem Physiol A Mol Integr Physiol. 159:75–81. doi:10.1016/j.cbpa.2011.01.020.

Uehara, M., K. Yashiro, S. Mamiya, J. Nishino, P. Chambon, P. Dolle, and Y. Sakai. 2007. CYP26A1 and CYP26C1 cooperatively regulate anterior-posterior patterning of the developing brain and the production of migratory cranial neural crest cells in the mouse. Developmental Biology. 302:399–411. doi:10.1016/j.ydbio.2006.09.045.

Untergasser, A., I. Cutcutache, T. Koressaar, J. Ye, B. C. Faircloth, M. Remm, and S. G. Rozen. 2012. Primer3—new capabilities and interfaces. Nucleic Acids Research. 40:e115–e115. doi:10.1093/nar/gks596.

U.S. Food and Drug Administration (FDA). 2006. Freedom of Information Summary Original New Animal Drug Application. NADA 141-258. Zilmax (Zilpaterol Hydrochloride). Type A Medicated Article for Cattle Fed in Confinement for Slaughter. Available from: http://www.fda.gov/downloads/AnimalVeterinary/Products/ ApprovedAnimalDrugProducts/FOIDrugSummaries/ ucm051412.pdf

U.S. Food and Drug Administration (FDA). 2020. Code of Federal Regulations. Title 21. Chapter I. Subchapter E. Part 558. Subpart B. Sec. 558.500 Ractopamine. Available from: https://www.accessdata.fda.gov/scripts/cdrh/cfdocs/cfcfr/CFRSearch.cfm?fr=558.500

Vasconcelos, J. T., R. J. Rathmann, R. R. Reuter, J. Leibovich, J. P. McMeniman, K. E. Hales, T. L. Covey, M. F. Miller, W. T. Nichols, and M. L. Galyean. 2008. Effects of duration of zilpaterol hydrochloride feeding and days on the finishing diet on feedlot cattle performance and carcass traits1. Journal of Animal Science. 86:2005–2015. doi:10.2527/jas.2008-1032.

Verhoeckx, K. C. M., R. P. Doornbos, J. V. D. Greef, R. F. Witkamp, and R. J. T. Rodenburg. 2005. Inhibitory effects of the β2-adrenergic receptor agonist zilpaterol on the LPS-induced production of TNF-α in vitro and in vivo. Journal of Veterinary Pharmacology and Therapeutics. 28:531–537. doi:https://doi.org/10.1111/j.1365-2885.2005.00691.x.

Vieux-Rochas, M., L. Coen, T. Sato, Y. Kurihara, Y. Gitton, O. Barbieri, K. L. Blay, G. Merlo, M. Ekker, H. Kurihara, P. Janvier, and G. Levi. 2007. Molecular Dynamics of

Retinoic Acid-Induced Craniofacial Malformations: Implications for the Origin of Gnathostome Jaws. PLoS ONE. 2. doi:10.1371/journal.pone.0000510.

Vitt, R., L. Weber, W. Zollitsch, S. J. Hörtenhuber, J. Baumgartner, K. Niebuhr, M. Piringer, I. Anders, K. Andre, I. Hennig-Pauka, M. Schönhart, and G. Schauberger. 2017. Modelled performance of energy saving air treatment devices to mitigate heat stress for confined livestock buildings in Central Europe. Biosystems Engineering. 164:85–97. doi:10.1016/j.biosystemseng.2017.09.013.

Volodina, O., S. Ganesan, S. C. Pearce, N. K. Gabler, L. H. Baumgard, R. P. Rhoads, and J. T. Selsby. 2017. Short-term heat stress alters redox balance in porcine skeletal muscle. Physiological Reports. 5:e13267. doi:https://doi.org/10.14814/phy2.13267.

Waldo, G. L., J. K. Northup, J. P. Perkins, and T. K. Harden. 1983. Characterization of an altered membrane form of the beta-adrenergic receptor produced during agonist-induced desensitization. Journal of Biological Chemistry. 258:13900–13908. doi:10.1016/S0021-9258(17)44003-8.

Walker, D. K., E. C. Titgemeyer, E. K. Sissom, K. R. Brown, J. J. Higgins, G. A. Andrews, and B. J. Johnson. 2007. Effects of steroidal implantation and ractopamine-HCl on nitrogen retention, blood metabolites and skeletal muscle gene expression in Holstein steers. Journal of Animal Physiology and Animal Nutrition. 91:439–447. doi:https://doi.org/10.1111/j.1439-0396.2007.00675.x.

Wang, J., X. Xue, Q. Liu, S. Zhang, M. Peng, J. Zhou, L. Chen, and F. Fang. 2019. Effects of duration of thermal stress on growth performance, serum oxidative stress indices, the expression and localization of ABCG2 and mitochondria ROS production of skeletal muscle, small intestine and immune organs in broilers. Journal of Thermal Biology. 85:102420. doi:10.1016/j.jtherbio.2019.102420.

Webb, B., and A. Sali. 2016. Comparative Protein Structure Modeling Using MODELLER. Current protocols in bioinformatics. 54:5.6.1-5.6.37. doi:10.1002/cpbi.3.

Wieczorek, D. 2013. Human facial dysostoses. Clinical genetics. 83:499–510. doi:https://doi.org/10.1111/cge.12123.

Williams, A. L., and B. L. Bohnsack. 2019. What's retinoic acid got to do with it? Retinoic acid regulation of the neural crest in craniofacial and ocular development. Genesis. 57:1–13. doi:10.1002/dvg.23308.

Winterholler, S. J., G. L. Parsons, C. D. Reinhardt, J. P. Hutcheson, W. T. Nichols, D. A. Yates, R. S. Swingle, and B. J. Johnson. 2007. Response to ractopamine-hydrogen chloride is similar in yearling steers across days on feed1. Journal of Animal Science. 85:413–419. doi:10.2527/jas.2006-555.

Wiszniak, S., F. E. Mackenzie, P. Anderson, S. Kabbara, C. Ruhrberg, and Q. Schwarz. 2015. Neural crest cell-derived VEGF promotes embryonic jaw extension. Proceedings of

the National Academy of Sciences of the United States of America. 112:6086–6091. doi:10.1073/pnas.1419368112.

Xie, J., L. Tang, L. Lu, L. Zhang, L. Xi, H.-C. Liu, J. Odle, and X. Luo. 2014. Differential Expression of Heat Shock Transcription Factors and Heat Shock Proteins after Acute and Chronic Heat Stress in Laying Chickens (Gallus gallus). PLOS ONE. 9:e102204. doi:10.1371/journal.pone.0102204.

Ye, X., M. Li, T. Hou, T. Gao, W. Zhu, and Y. Yang. 2016. Sirtuins in glucose and lipid metabolism. Oncotarget. 8:1845–1859. doi:10.18632/oncotarget.12157.

Yépez, V. A., L. S. Kremer, A. Iuso, M. Gusic, R. Kopajtich, E. Koňaříkova, A. Nadel, L. Wachutka, H. Prokisch, and J. Gagneur. 2018. OCR-Stats: Robust estimation and statistical testing of mitochondrial respiration activities using seahorse xf analyzer. PLoS ONE. 13:1–18. doi:10.1371/journal.pone.0199938.

Zuo, J., M. Xu, Y. A. Abdullahi, L. Ma, Z. Zhang, and D. Feng. 2015. Constant heat stress reduces skeletal muscle protein deposition in broilers. Journal of the Science of Food and Agriculture. 95:429–436. doi:https://doi.org/10.1002/jsfa.6749.